

Quantum Cascade Laser for Spectroscopic Gas Detection

Bjørn Sletbakk

Master of Science in Electronics
Submission date: August 2007
Supervisor: Astrid Aksnes, IET

Problem Description

Norsk Elektro Optikk AS has developed a series of gas detection equipment based on tunable diode lasers and single line spectroscopy. Some gases have few or no absorption lines in the wavelength area where there are available diode lasers. This means that some gases can not be detected today based on 'standard' tunable diode lasers. Quantum cascade lasers (QCL) make it possible to measure at wavelengths much greater than 5 μ m. These lasers are beginning to become stable and reliable components. NEO wishes to test QCL for measurement of gases in ranges where it has been difficult to measure before.

This master thesis will examine the QCL characteristics and construct a laboratory setup that can be implemented in spectroscopic trace gas detection. The setup will be built with a QCL, a detector and other necessary electronics. Experiments will be performed to control the laser temperature and drive current to enable the QCL to be used in spectroscopic measurements.

Assignment given: 25. January 2007
Supervisor: Astrid Aksnes, IET

Quantum Cascade Laser for Spectroscopic Gas Detection

Author: Bjørn Sletbakk

Supervisor: Astrid Aksnes

Norwegian University of Science and Technology
Faculty of Information Technology, Mathematics
and Electrical Engineering
Department of Electrical Engineering and Tele Communications

July 2007



NTNU
Norwegian University of
Science and Technology

Abstract

In this project it has been focused on the use of a 7.42 μm , 4 mW Quantum Cascade Laser in trace gas detection spectroscopy. Norsk Elektro Optikk (NEO) is in possession of a Nanoplus G2102/DFB2/5-12 QCL laser, that can be used in spectroscopic detection of H_2O , CO_2 and SO_2 .

It has been attempted to construct a setup that can be used for spectroscopic measurements using a self constructed current driver module to produce current pulses for the QCL. The QCL is operated in pulsed mode, with pulses of <500 ns width, and a 1 kHz pulse repetition frequency. Temperature control of the laser has been conducted with a LaserGas II SP monitor module, and temperature has been kept at 280 K during testing.

Initially, various test have been conducted to ensure the general functionality of the driver module, and to avoid damage to the QCL. Two different solutions for the transmission line from the driver to the QCL have also been examined, and it has been concluded that the current pulses supplied to the laser are of good quality with minor broadening and short rise/fall times. Furthermore an I-V characteristic for the laser has been produced by incrementing the laser driving current, and measuring the corresponding laser voltage.

Measurements of the laser output power have been conducted using a CaF_2 collimating lens to focus the laser beam onto a PVI-2TE-8 Vigo photovoltaic detector from Vigo Systems S.A. It has proved difficult to obtain a good signal from the detector, with the maximum voltage measured across a 50 Ω shunt resistor being 3 mV. This is 100-200 mV less than what should be expected.

Various methods of noise reduction have been applied to improve the detected signal, none have however provided any noticeable improvements. Several possible reasons for the generally low output have been examined.

Preface

This project has been conducted for Norsk Elektrooptikk AS (NEO), at the Department of Electrical Engineering and Tele Communications (IET) of NTNU. All testing, modifications, and laboratory work has been conducted at laboratories at NTNU. First and foremost I would like to thank my supervisor, Associate Professor Astrid Aksnes, for all her guidance throughout the project, and for always taking the time to give me thorough help and feedback. I will also thank Ivar Linnerud and the people at NEO for giving me the opportunity to do the project, for providing equipment, and for giving guidance when needed.

Last, but not least, I would like to thank the members of Team Pettersen for keeping my spirits high throughout the project.

Contents

I	Introduction	1
II	Theory	3
1	Near and Mid-IR spectroscopy	3
2	The Quantum Cascade laser	4
2.1	Development and characteristics	4
2.2	Pulsed and Continuous Wave (CW) operation	6
2.3	Distributed feedback	7
2.4	H ₂ O, CO ₂ and SO ₂ absorption	9
3	Photodetectors	10
4	Electrical noise	12
4.1	Component noise	13
4.2	Coupling noise	14
III	Instrumentation and setup	17
5	Signal generation	18
6	Lasergas II	20
7	The laser driver module	21
7.1	PCO 7120	22
7.2	NEO design driver module	22
7.2.1	Driver components	25
7.2.2	Modifications of the NEO design driver module	26
IV	Measurements and results	29
8	Testing of the driver modules with laser equivalent	29
8.1	PCO 7120	30
8.2	NEO design	31
8.2.1	PCB mount	32
8.2.2	Twisted pair mount	33
8.2.3	Copper strip mount	34

9	Testing with the QCL	35
9.1	Verification of polarity	35
9.2	Producing the I-V characteristics of the QCL	38
9.3	Conducting measurements with the Vigo detector	38
V	Discussion of results	43
VI	Conclusions	45
VII	Outlook and future work	47
A	Datasheet for the QCL	51
B	Datasheet for the Vigo detector	54
C	Datasheet for the BCT03C6V2 Zener diode	57
D	NEO design driver module circuit	62
E	PCO 7120 information	63
F	Additional images of zener equivalent measurements	67
G	Comparison of I-V graphs for zener equivalent	70
H	Laboratory setup image	71
I	Noise measurements	72
J	Labview block diagram	74

List of Figures

2.1	Transmission electron microscope image of several periods in a QCL structure. Figure from [9]	5
2.2	Schematic showing the quantum well confinement and periodic structure of the QCL. Figure from [6]	6
2.3	Multiple photon emissions as the electrons cascade through the stages.	6
2.4	Bragg grating in a waveguide, reflecting λ_B while other frequencies are transmitted. Figure from [13].	8
2.5	View of a junction-down mounted QC-DFB laser soldered on a diamond plate. The lateral i-InP layer is partially removed to show the DFB grating etched in the InGaAs waveguide layer. Figure from [12].	8
2.6	Scanning of the laser across the absorption line. Figure from [1]	8
2.7	Peak output power of QCL vs. supplied current. Lasing starts at 2.15 A. Operation current of 2.6 A yields 4 mW peak output power.	9
2.8	Absorption lines for SO ₂ at 4 and around 7.35 μm . Figure from [1]	10
2.9	Absorption lines for H ₂ O in the near- and mid-IR spectra. The latter being about 12x stronger. Figure from [1]	10
3.10	Photovoltaic effect. Voltage induced by photons striking a P-N junction. (figure from [25])	11
3.11	Radiation is focused onto the detector chip by the resin. The width of the radiation window is approximately 1 mm. The width of the chip is approximately 0.1 mm.	12
4.12	50 Ω termination resistors used in the NEO driver design (figure 7.20). R ₁₆ is soldered on the PCB for convenience.	15
4.13	Model of transmission line with parasitic capacitance, inductance and resistance.	15
4.14	The laboratory setup with the driver module, its signal and DC inputs, the QCL with its LaserGas II temperature controller, the detector and its PSU for Peltier cooling, the oscilloscope, and a possible gas sample cell in the QCL ray path.	17
4.15	The actual tube (left), showing the QCL and a cut out window for accessibility. A cross section of the tube (right), showing the placement of the collimating lens.	18
5.16	The LabView front panel interface used for generation of driver module input signals.	19
6.17	LaserGas II SB monitor (left) and the software interface for monitoring different variables (right).	20
6.18	The laser mount showing the QCL, heat sink and Peltier element. Note that the aluminium tube has been removed.	21
7.19	PCO 7120 with outputs, inputs and current limiting resistor.	23
7.20	The initial driver design from NEO used in [22]	23
7.21	Sketch of I_{laser} vs. the voltage of the current mirror output.	24

7.22	Addition of six ceramic capacitors between the power rail and ground. Also showing modification of R_8 and R_9	28
8.23	The QCL equivalent composed of a resistor in series with a reverse biased Zener diode.	29
8.24	Theoretical outline of the laser equivalent I-V graphs. <i>b)</i> shows the contribution of the resistor, <i>a)</i> shows the contribution of the reverse biased Zener diode, and <i>c)</i> shows the superposition of the two, representing the total laser equivalent. <i>d)</i> shows the theoretical I-V characteristic of the QCL, which <i>c)</i> is supposed to resemble.	30
8.25	PCO 7120 output across a 1Ω resistor. The voltage value is halved because of coax termination to the oscilloscope, making the real voltage 5 V. This corresponds to 5 A across a 1Ω resistor.	31
8.26	Zener diode mounted directly on PCB. Also showing coax cable to oscilloscope, and 50Ω terminating resistor (blue)	32
8.27	Output from PCB with laser equivalent zener diode mounted on PCB. Peak voltage of 396 mV corresponding to 2.4 A current magnitude. Pulse width of 500 ns.	33
8.28	Zener diode mounted at the end of 30 cm long twisted copper wires.	34
8.29	Output from PCB with laser equivalent zener diode mounted at the end of 30 cm long TP copper wires. Peak voltage of 396 mV corresponding to 2.4 A current magnitude. Pulse width of 500 ns.	35
8.30	Zener diode mounted at the end of two 30 cm long, 2.5 cm wide copper strips. Paper isolation in between. The bottom (positive) strip is not showing.	35
8.31	Output from PCB with laser equivalent zener diode mounted at the end of 30 cm long, 2.5 cm wide copper strips. Peak voltage of 396 mV corresponding to 2.4 A current magnitude. Pulse width of 500 ns.	36
9.32	I-V characteristics measured for the zener diode alone (red), and the QCL and zener diode in parallel (green). The zener breakdown at 6.2 V is clearly visible.	37
9.33	Reference voltage corresponding to a peak current magnitude of 2.7 A. Voltage measured across the reference resistor, R_{15} in the NEO design driver circuit.	38
9.34	I-V characteristics of the QCL mounted at the end of 30 cm long, 2.5 cm wide copper strips. Voltage measured at intervals of 0.1 A. The data are plotted in GNUplot.	39
9.35	Pictures showing the comparison of detected laser signal (left), and object blocking the laser path (right). Resolution is 100 ns per square on the x-axis, and 5 mV per square on y-axis.	40
9.36	Top view of the QCL tube and detector placement. Showing a slightly better detection with the detector being a small distance off the center alignment. Distance from tube to detector plate is kept fixed.	42
E.37	Image of the PCO 7120 and its input and output terminals.	66
F.38	Zener mounted on PCB. Current peak of 2.2 A	67

F.39 Zener mounted on PCB. Current peak of 2.6 A	67
F.40 Zener mounted with TP wires. Current peak of 2.2 A	68
F.41 Zener mounted with TP wires. Current peak of 2.6 A	68
F.42 Zener mounted with copper strip. Current peak of 2.2 A	69
F.43 Zener mounted with copper strip. Current peak of 2.6 A	69
G.44 Comparison of I-V graphs for zener mounted on PCB and on copper strip.	70
H.45 Picture of the laboratory setup with detector close to QCL mount and aluminium tube removed.	71
I.46 Image of detector noise. Also showing the triggering signal of the detector.	72
I.47 Fluctuation in ground potential on PCB.	72
I.48 Fluctuation in ground potential on PCB.	73
J.49 The Labview block diagram used for pulse generation.	74

List of Tables

- 7.1 Component types and values used in 7.20. C is capacitor, R is resistor, Q represents a transistor and D represents a diode. 26
- 7.2 A table showing all the different circuit configurations of the NEO design. Each row in the table corresponds to one test configuration. *Testing order* states the order in which the configurations were tested. This is chosen for practical purposes, so that the least amount of components would be changed between each configuration. For each set up, V_{in} was constant and supplied by the signal generator. V_{out} is the voltage across R_{15} . I_{laser} is V_{out} divided by the value of R_{15} . V_A is the supply voltage ranging from 15-25 V. An X in the table signifies that this value was measured, or in the case of I_{laser} , calculated from V_{out} . NC means not connected, while C means connected. C is capacitor, R is resistor, Q represents a transistor and D represents a diode. 27

Part I

Introduction

Norsk Elektrooptik AS have developed a series of gas detectors based on tunable diode lasers and single line spectroscopy. Some gases have few or no absorption lines in the wavelength range where there are available diode lasers.

Quantum cascade lasers makes it possible to conduct measurements on wavelengths above 5 μm , and are starting to become a reliable component. NEO wishes to test quantum cascade lasers for measurements on gases that have been inaccessible using conventional diode lasers.

In this project it has been attempted to produce a functional laboratory setup for spectroscopic gas detection using a G2102/DFB2/5-12 quantum cascade laser from Nanoplus. This QCL is emitting at 7.42 μm in the IR region, which makes it applicable for detection of H_2O and CO_2 in air, and SO_2 in a cell.

Gas detection by spectroscopy is based on the Beer-Lambert's law, which states that the amount of laser power absorbed by a gas is proportional to its concentration and path length of the beam through the sample. This makes it possible to measure the received power, and calculate gas concentration from the known output power of the laser.

During this project the operation of the QCL will be conducted in pulsed mode. This makes it necessary to implement a current pulse driver module that deliver short accurate current pulses of a magnitude of 0-2.8 A. The pulses should have a width of <500 ns and a pulse repetition frequency (PRF) of 1 kHz to avoid excessive heating of the laser.

Temperature control of the laser during operation will be done by the LaserGas II SP monitor module that NEO uses in their industrial spectroscopic gas detection applications.

Detection of the received laser power will be done with a 2 stage, TE cooled PVI-2TE-8 photovoltaic detector from Vigo Systems S.A.

The project is a continuation of my earlier student project. In the student project it was focused on different ways of implementing the laser current driver module circuitry.

Part II

Theory

1 Near and Mid-IR spectroscopy

Spectroscopy in its simplest form is a way of detecting gases in an environment by exposing them to electromagnetic fields. A light source, commonly a laser, will emit light with a given frequency at a known intensity, and a detector at the other side of a sample cell will detect the received intensity. Spectroscopy utilizes the fact that a given molecule absorbs and scatters light differently at different frequencies. Because of this, each molecule has its own unique absorption spectrum, which can be used to identify this molecule in an environment. Absorption spectra for many different molecules and substances is stored in a universal database called, HITRAN (High-resolution transmission molecular absorption database). When trying to detect a concentration of a given molecule in a sample cell, it is important to first find a frequency at which this molecule has a large absorption line. Secondly there should be no other molecules in the sample with absorption lines at the same frequency. Lines are broadened with increasing temperature, however at low pressure conditions, most absorption lines are quite narrow. Between $0.01 - 0.1 \text{ [cm}^{-1}]$ [7]. Line width is usually denoted with this wave number, rather than wave length. The wave number is simply the inverse of the wave length. Multiplied with a factor 10.000 to convert from $[\mu\text{m}]$ to $[\text{cm}^{-1}]$ respectively.

To detect the molecule in question, a laser with the appropriate wavelength emission and tunability option, should be frequency scanned over the selected absorption line. By detecting the received intensity and comparing it to the emitted intensity, the concentration of the molecule can be calculated using the Beer-Lambert law (equation 1.1) [26, 24, 7].

$$I(f) = I_0(f)e^{-\alpha(f) \cdot C \cdot L} \quad (1.1)$$

This law states that for a given path length, the received intensity is equal to the emitted intensity multiplied with a damping factor of $e^{-\alpha(f) \cdot C \cdot L}$. In this expression L represents the path length, α is the optical absorption coefficient and C is the concentration of the gas molecules in question.

Commonly, tunable diode lasers are used in spectroscopic measurements. However their emission wavelengths are limited to the near IR spectrum, of about $1.25 - 2 \mu\text{m}$ [11], and strongly depend upon the band gap energy of the laser material. Many of the trace gas molecules however have absorption lines that are as much as 100x stronger [1] in the mid-far IR range. This makes it desirable to use laser technology with emission at these frequencies for greater line selectivity and ultimately detection of smaller gas concentrations.

The Beer-Lambert law can also be expressed as [7]:

$$I(f) = I_0(f)e^{-S \cdot g(f) \cdot C \cdot L} \quad (1.2)$$

Where S is the line strength of the given line [cm/molecule], and $g(f)$ is the line shape function. A Lorentzian line shape function is commonly used as an approximation [4]. The absorption coefficient can be identified in (equation 1.2) as: $\alpha(\nu) = S \cdot g(\nu - \nu_0)$. $g(\nu - \nu_0)$ is the normalized line shape function with center wave number ν_0 .

2 The Quantum Cascade laser

2.1 Development and characteristics

The Quantum cascade laser (QCL) technology was discovered and demonstrated for the first time by Jerome Faist, Federico Capasso, Deborah Sivco, Carlo Sirtori, Albert Hutchinson, Claire Gmachl, and Alfred Cho at Bell Laboratories in 1994. This initial QCL was emitting at 4.3 μm , at cryogenic temperatures and was operated solely in pulsed mode [10]. Since its first demonstration the features of QCL technology has been greatly improved, and today room temperature pulsed mode operation, as well as cryogenic continuous wave operation can be achieved. The Quantum cascade lasers of today have the ability to cover wavelengths of the entire mid-far IR spectrum, ranging from 3.5-24 μm [5]. Because of the ability to emit narrow banded light in the mid-IR spectrum, with optical output power of several Watts, the QCL has proved to be advantageous for use in trace gas spectroscopy. QCL-based trace gas sensors utilizing different detection schemes are capable of quantifying optical absorbance down to 10^{-9} cm^{-1} in the mid-IR fingerprint region (for fundamental molecular absorption bands) [27].

The Quantum cascade laser technology differs from conventional laser technology in a few important ways. In a conventional bulk semiconductor crystal the electrons can occupy either the valence band or the conduction band. Between these bands, the crystal has a band gap which the electrons are not permitted to occupy. The photon emission in such crystals arise from electrons being excited across the bandgap by an external pumping source, and subsequently by stimulation, transition back across the band gap. In the valence band, the electrons recombine with holes, and the transition energy of one single electron is emitted as a photon. In this case the energy of the emitted photon is equal to the energy band gap of the given semiconductor material.

The QCL however does not rely on electrons transitioning from the conduction band to the valence band of a given atom. Instead it is based upon the quantum physical effects that arise when electrons are confined in micro structure quantum wells. As the name implies the QCL consists of several cascading stages, each consisting of many ultra thin layers of alloy metals. Usually (Al, Ga, As, In). An electron microscope image of the layering within a QCL can be viewed in figure 2.1.

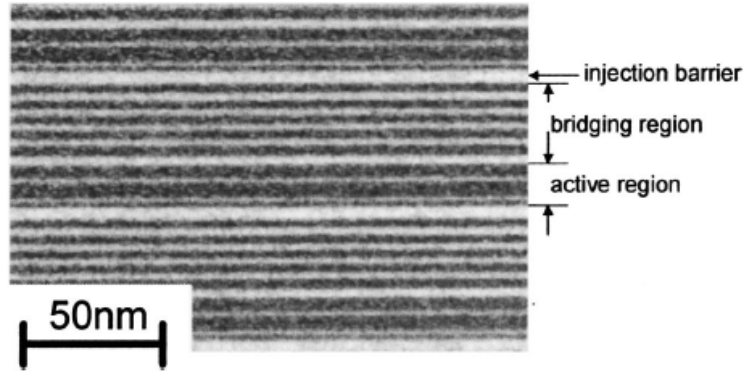


Figure 2.1: Transmission electron microscope image of several periods in a QCL structure. Figure from [9]

The different layers within one period of the laser material is only a few atoms thick and provide sharp atomically flat interfaces. Within these small dimensions the electrons obtain quantum physical behavior, and the rapidly varying material composition gives a varying electrical potential in the transitional direction of the laser material. This variation in electric potential is called quantum well confinement, and leads to a splitting of the band of permitted energy into several sub-bands, each with different momentum (figure 2.2). [8].

By carefully choosing the different materials as well as the thickness of the layers and the externally applied electric field, it is possible to align a sub-band minima in one period of the laser with a sub-band maxima in the following period. Between each quantum well an injector region is placed. The purpose of these regions are to confine the electrons and inject them from the bottom of the quantum well in period i to the top of the well in period $i + 1$ (figure 2.2).

From this the concept of the QCL can be explained. Each given electron will experience an optical transition between sub-bands in one period of the laser, emitting one photon, before tunneling into the next period and making another optical transition with a coherent emission. Each electron transversing the laser will emit n photons corresponding to the n stages of the laser (figure 2.3). This makes it possible to achieve high output power compared to conventional diode lasers, as these will only emit one photon per transmitted electron. A typical QCL will consist of between 25 and 75 stages [15], depending on desired laser wavelength, output power and material composition. Because the emission wavelength is decided by material composition rather than material characteristics, it is possible to use reliable, well understood semiconductor materials in the QCL construction. And the same materials can be used to construct different wavelength lasers.

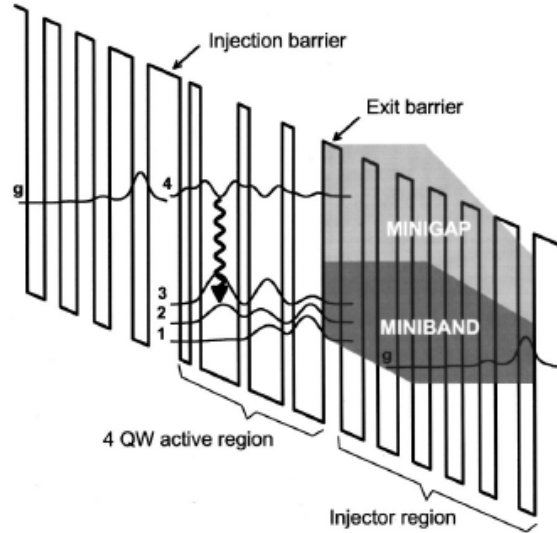


Figure 2.2: Schematic showing the quantum well confinement and periodic structure of the QCL. Figure from [6]

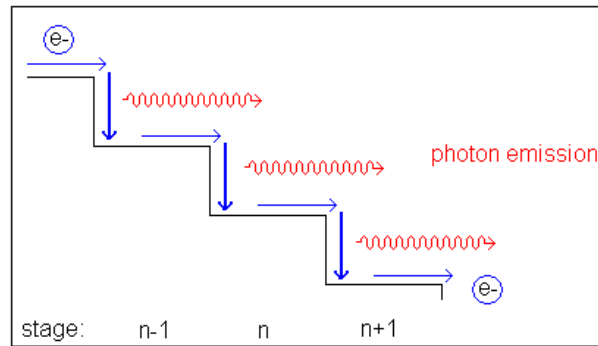


Figure 2.3: Multiple photon emissions as the electrons cascade through the stages.

2.2 Pulsed and Continuous Wave (CW) operation

Because each electron emits n photons upon moving through the n stages of the QCL, it follows that the QCL has natural intrinsic high power qualities, when compared to conventional diode lasers. As a result of this, heat dissipation in the QCL can easily be a problem, and therefore operation of QC lasers in continuous mode (CW) requires a cryogenic testing environment. Usually with liquid nitrogen cooling.

Pulsed QC lasers have the advantage of being able to be operated at room temperature with the use of thermoelectric cooling. However, they suffer a disadvantage of

line broadening effects, when compared to CW operated lasers. The line broadening of pulsed lasers arise from the concept of thermal chirping, which is a thermally induced, gradual change in frequency over time. While this is a problem in applications that require strong line selectivity, pulsed operation will be adequate in other less requiring applications, such as measurements at well-isolated absorption lines or lines that are strongly pressure-broadened [27]. Pulsed lasers also have greater beam divergence, limiting the effective sample path length.

2.3 Distributed feedback

In trace gas spectroscopy it is imperative that the QCL emission frequency can be matched exactly to the fundamental absorption bands of the trace gas in question. Distributed feedback QC lasers have the ability to offer single frequency, tunable light emission and continuous mode operation has been successfully demonstrated for wavelengths ranging from 4.6-11.8 μm over extensive periods of time [12].

The distributed feedback laser uses a Bragg grating in conjunction with the laser cavity (see figure 2.5). A Bragg grating consists of a waveguide with a perturbed refractive index, varying periodically along the direction of light propagation. Upon entering the grating, a narrow band of the incident light is reflected and added in phase from each of the different index variation periods (see figure 2.4). This wavelength is thereby effectively separated from the other frequency components, which are transmitted through the waveguide. The reflected wavelength is known as the Bragg wavelength, λ_B , and can be manipulated by changing the grating period, Λ . The Bragg condition satisfies:

$$\lambda_B = 2n_{eff}\Lambda \quad (2.3)$$

n_{eff} is the effective modal index of the waveguide. Each reflection is in phase with the next one at λ_B [13].

Changes in the grating properties, such as strain, temperature or polarization will effectively change the Bragg wavelength. Manipulation of these properties can then be used to tune or scan a QCL output wavelength across trace gas absorption lines (figure 2.6).

In this project the QCL is a distributed feedback G2102/DFB2/5-12 laser developed by Nanoplus (see appendix A). This laser is emitting at 7.42 μm , and will be operated in pulsed mode. At 7.42 μm it is possible, and desired, to measure H_2O and CO_2 in air, and SO_2 in a cell.

Figure 2.7 shows the peak output power in mW as a function of the supplied current pulses to the QCL. It is evident that we need a current of at least 2.15 A to initiate lasing. At the suggested operation current of 2.6 A, the peak output power should be 4 mW. Of course the mean output power, using short pulses with relatively slow pulse repetition frequency (PRF), will be considerably lower. This will ease the temperature controlling of the QCL and help avoid overheating. The increase in peak output power between the threshold current and the operation current is approximately linear.

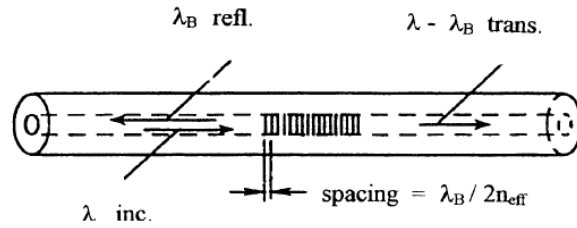


Figure 2.4: Bragg grating in a waveguide, reflecting λ_B while other frequencies are transmitted. Figure from [13].

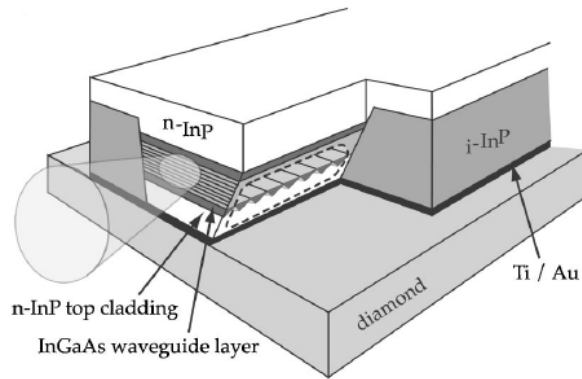


Figure 2.5: View of a junction-down mounted QC-DFB laser soldered on a diamond plate. The lateral i-InP layer is partially removed to show the DFB grating etched in the InGaAs waveguide layer. Figure from [12].

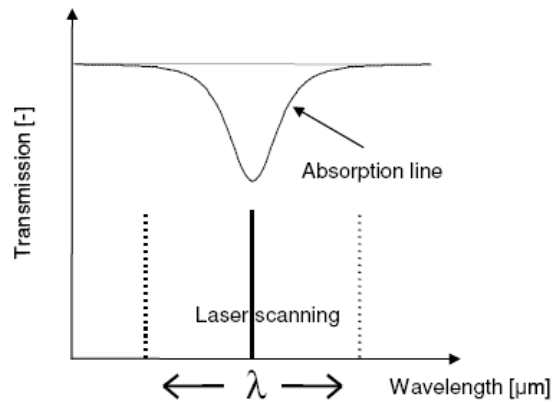


Figure 2.6: Scanning of the laser across the absorption line. Figure from [1]

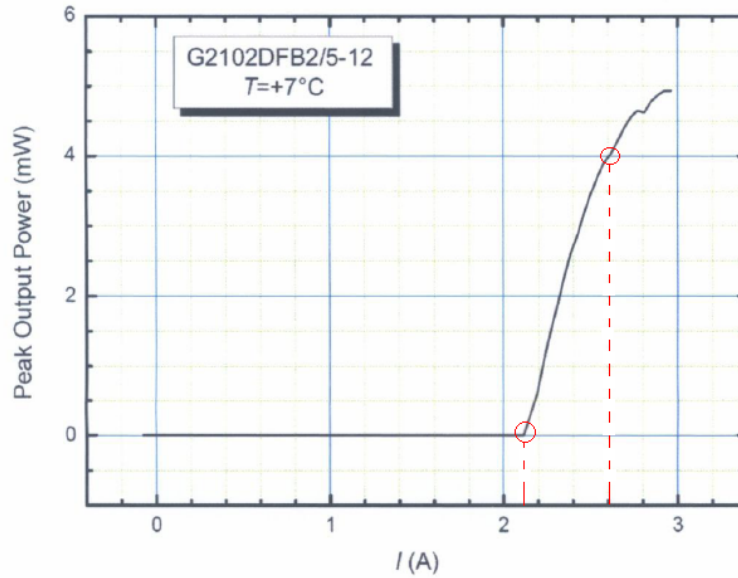


Figure 2.7: Peak output power of QCL vs. supplied current. Lasing starts at 2.15 A. Operation current of 2.6 A yields 4 mW peak output power.

2.4 H₂O, CO₂ and SO₂ absorption

While the near-IR spectrum is commonly used to detect gaseous chemicals, the absorption in this spectrum is often due to overtone or combination bands. Because of this, the magnitude of the absorption lines are generally weaker, often as much as 2-100x [1], than the mid-IR fundamental absorption bands. This affects the detection limits of the chemicals negatively.

In the 7.42 μm wavelength vicinity there are particularly three gases that have strong absorption lines. The SO₂ molecule is particularly interesting because it has generally low sensitivity for detection. It has two strong absorption lines, one at 4 μm and another at about 7.35 μm [1]. The latter being the most interesting in this project. From figure 2.8 we can see that the absorption line around 7.35 μm is somewhat 50 times stronger than the first absorption line. Also H₂O (figure 2.9) and CO₂ has more prominent absorption lines in the mid-IR than in the near-IR spectrum. This makes them favorable for detection at QC laser wavelengths.

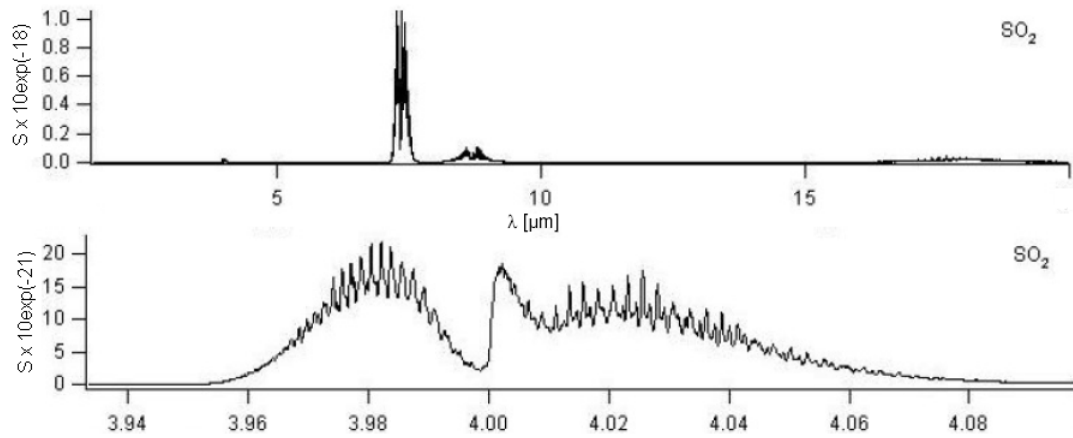


Figure 2.8: Absorption lines for SO_2 at 4 and around $7.35 \mu\text{m}$. Figure from [1]

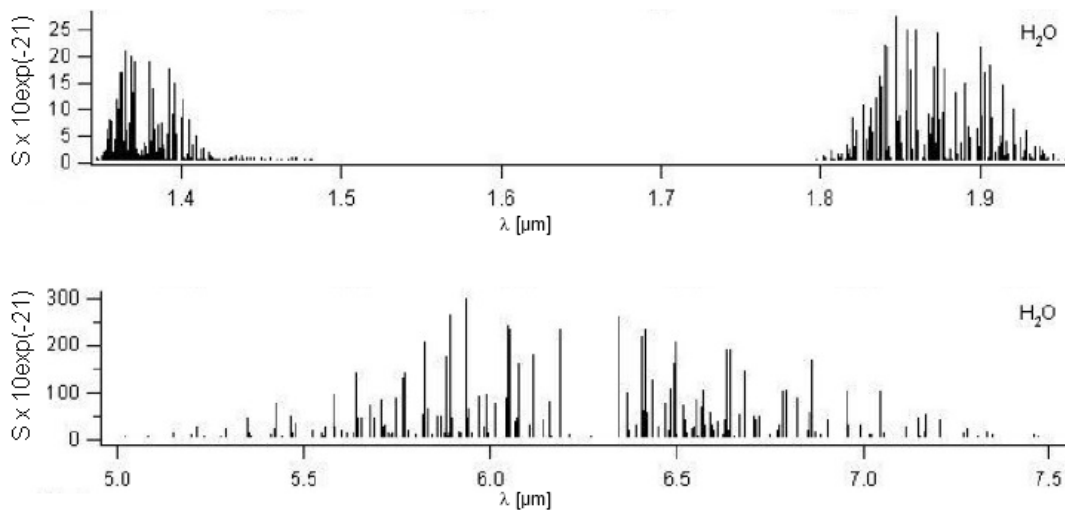


Figure 2.9: Absorption lines for H_2O in the near- and mid-IR spectra. The latter being about 12x stronger. Figure from [1]

3 Photodetectors

Photodetector is a common description for all light or electromagnetic energy detecting devices. Generally photodetectors are separated into either photovoltaic or photoconductive mode devices. *Photoconductive* detectors are operated on the basis of photoconductivity, which is an optical and electrical phenomenon in semiconductor devices. The concept arises as the semiconductor material absorbs electromagnetic radiation i.e. visible light, UV light, IR light or gamma radiation, and experiences an increased

conductivity. When light with sufficient energy strikes the semiconductor, electrons are excited across the band gap into the conduction band. A bias voltage and a load resistor is in turn utilized in series with the semiconductor, and the degree of increased conductivity can be measured by the voltage drop across the resistor. More information on photoconductivity can be found in [24].

The detector used in this project is a *photovoltaic* IR detector from Vigo Systems S.A. (see appendix B). Photovoltaic detectors contain a P-N junction. When a photon strikes the semiconductor electron-hole pairs are excited, and separated by the P-N junction. This in turn creates an electric potential that can be measured. The process can be viewed in figure 3.10.

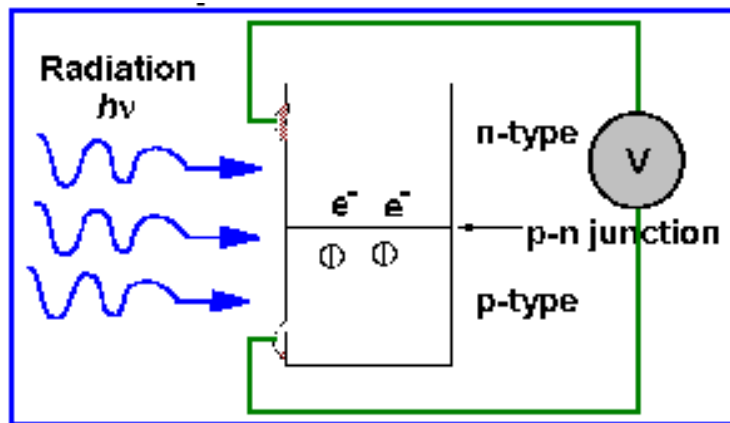


Figure 3.10: Photovoltaic effect. Voltage induced by photons striking a P-N junction. (figure from [25])

The Vigo detector is constructed to have peak sensitivity at $8 \mu\text{m}$. This is achieved by using variable gap (Hg,Cd,Zn)Te semiconductors, and optimize doping concentrations. In addition, the Vigo detector is constructed using a light focusing resin, that covers the detector chip entirely (see figure 3.11). This resin has refracting abilities that enable more light to strike a smaller detector chip. The ability to focus more light onto a smaller chip has some advantages. Primarily, its sensitivity increases because of the higher intensity of radiation striking the area. This excites more electron-hole pairs, and generates a greater voltage difference. Secondly, the internal parasitic capacitance of the detector decreases, as it is highly dependent on the detector area.

A problem with the Vigo detector is that it is more easily saturated, because of the high intensity of light striking the small chip.

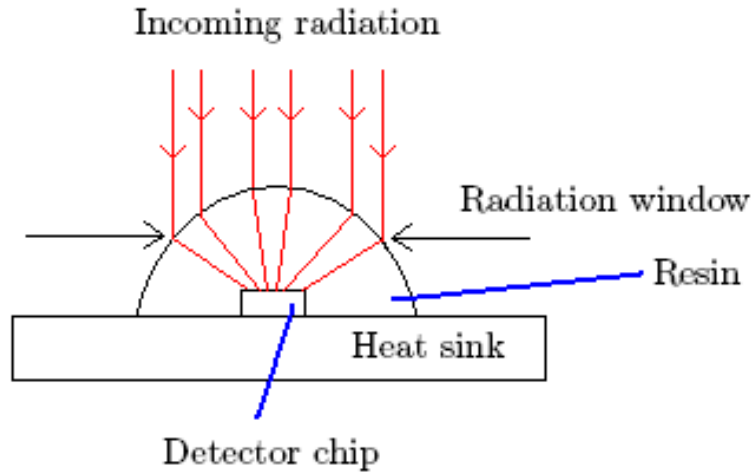


Figure 3.11: Radiation is focused onto the detector chip by the resin. The width of the radiation window is approximately 1 mm. The width of the chip is approximately 0.1 mm.

4 Electrical noise

The phenomenon of electrical noise is of great importance in many analogue designs. Especially those that deal with RF signals and high switching times. In this project in particular, noise reduction proved to be a significant part of getting the laser driver circuit to deliver the necessary current pulse quality to the laser. The following paragraph will discuss some common sources of electrical noise, how to improve the signal to noise ratio, or avoid the different noise components all together.

Electrical noise in a given signal can be described as: Random, and to a certain degree unpredictable, electronic charges that appear in addition to the stable signal [23]. Nonlinearities in components are not considered electrical noise.

In general, electrical noise is described as either *component noise*, *coupling noise*, or a combination of the two. They both have the undesired effect that they throw off measurements according to expected, calculated, or simulated results. There are no strict definitions as to what categories of noise subside under either component noise or coupling noise, yet the divisions are quite established.

The most common sources of electronic noise belonging to each of the two categories as follows. List from [23]:

Component noise

- Thermal noise
- Shot noise

- $\frac{1}{f}$ noise or flicker noise
- Popcorn noise

Coupling noise

- Common impedance
- Parasitic capacitance
- Parasitic inductance
- Parasitic resistance
- Capacitive coupling
- Inductive coupling
- Electromagnetic radiation

4.1 Component noise

Thermal noise is generated in all components by thermal agitation of electrons in a conductor. The definition of thermal noise power is given by [3]:

$$P = kT\Delta f \quad (4.4)$$

Where k is Boltzmann's constant in Joules per Kelvin, T is the conductor temperature in Kelvin and Δf is the bandwidth in Hertz. It is notable that thermal noise power, per Hertz, is equal throughout the frequency spectrum.

Using 4.4 and applying Ohm's law, it follows that thermal noise in the real part of an impedance with resistance R , equals:

$$E = \sqrt{4kTR\Delta f} \quad (4.5)$$

Thermal noise is also referred to as *Johnson noise*.

Shot noise is noise caused by random fluctuations in the motion of charge carriers in a conductor [3]. The shot noise current can be described as [23]:

$$I_{sh} = \sqrt{2qI_{DC}\Delta f} \quad (4.6)$$

q is the elemental charge, I_{DC} is the average current through the device and Δf is the bandwidth. Shot noise follow a Poisson distribution, where I_{sh} is the standard deviation of the current fluctuations [21].

Flicker noise, also referred to as $\frac{1}{f}$ noise, is generally more dominant in low frequency circuits. Mostly due to suppression by white noise at higher frequencies. It arises in electronic components when a direct current is applied. It has a power spectral density proportional to $\frac{1}{f}$, hence the name. A thorough coverage of 1/f noise can be found in [14].

Popcorn noise, also referred to as burst noise, or Random telegraph signals, is a discrete modulation of the channel current in semi-conductor devices caused by the capture and emission of a channel carrier [18]. It generally consists of frequencies in the audio range, and the name is derived from popping noises that may appear from this type of noise in audio systems. Popcorn noise is most likely to be observed in transistors with small gate areas [17].

During the further development of this project the effect of component noise on the measurements have been disregarded for two reasons. Primarily, the magnitude of such noise is likely to effect the results to a much smaller degree than coupling noise, and should not have a great impact on the sensitivity or the required signal quality of the circuit. Secondly, the effects of component noise are not easily compensated, given the set selection of components and equipment that have been used in this project. Also, to identify and compensate for component noise, it is imperative to first identify and remove the coupling noise.

4.2 Coupling noise

Coupling noise can generally be contributed to the design and layout of the circuitry. It is greatly affected by the placing of the circuit components in reference to each other, in reference to the power rail, and in reference to the ground plane of the circuit. The width, length and spacing of all wiring and transmission lines also contribute greatly to the generated coupling noise. There are several effects that contribute to the coupling noise of the circuit.

Common impedance noise can arise when two or more signals share a common lead to a ground reference. This means that the signals are coupled by a common impedance to ground. In the case where one of these signals has an alternating current, and thereby an alternating voltage at the ground connection through the impedance, the ground voltage for the other signal will alternate as well.

A comprehensive derivation of common impedance noise from the transmission line equations can be found in [19].

When working with transmission lines in high frequency circuits and applications, the approximation of lossless transmission lines proves very inaccurate. It is mandatory that the impedance of the transmission line is matched to the impedance of the load. If these are not matched accurately to each other there will be multiple signal reflections between the transmission line and the load, resulting in signal distortion and power loss. Most coax cable transmission lines, including the ones used in this project, have a characteristic impedance of 50 Ω . An expression for the *reflection coefficient* can be written as follows:

$$\Gamma = \frac{R_L - Z_0}{R_L + Z_0} \quad (4.7)$$

With R_L being the load impedance, and Z_0 being the transmission lines' characteristic impedance. It is evident that this expression takes a value between 1 and

-1, being 0 when the impedances are matched. So for a coax cable with characteristic impedance equal to $50\ \Omega$, a $50\ \Omega$ termination on the load should be used.

In the design in this project the terminating $50\ \Omega$ resistors has another major impact. They reduce the voltage that is measured across the output terminal by half. This must be compensated by multiplying the measured voltage by 2 to find the actual voltage across the laser terminals at any given time. This can be understood from figure 4.12.

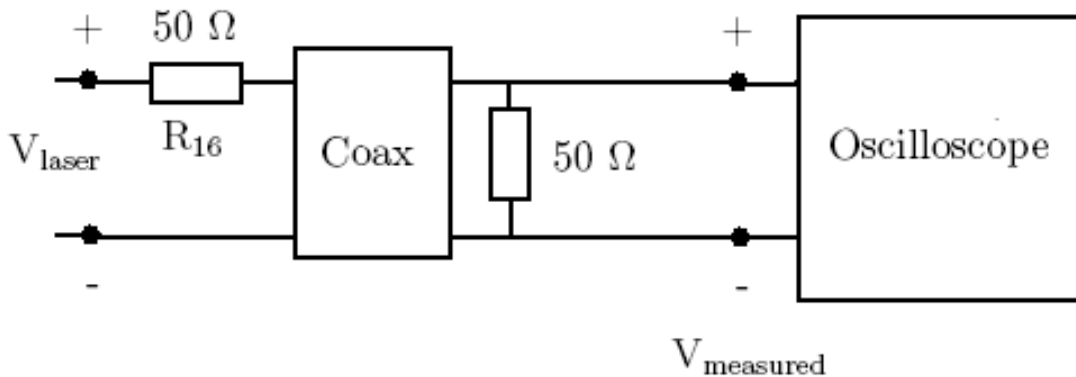


Figure 4.12: $50\ \Omega$ termination resistors used in the NEO driver design (figure 7.20). R_{16} is soldered on the PCB for convenience.

It is clear that V_{measured} will be half of V_{laser} , as the voltage drop is the same across both $50\ \Omega$ resistors. For more details on transmission lines, load matching and termination, see [2] and [20].

Any real life transmission line can be modeled as two leads containing a parasitic inductance, a parasitic capacitance, and an effective resistance (see figure 4.13).

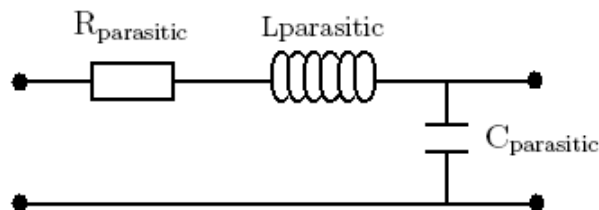


Figure 4.13: Model of transmission line with parasitic capacitance, inductance and resistance.

Parasitic capacitance is capacitance that is not taken into consideration when considering ideal circuit elements. Parasitic capacitance exist to some degree between

all conducting surfaces that have a voltage difference and are separated by a dielectricum. Whenever a parasitic capacitance are present it will be charged during operation, leading to deviating voltage levels in surrounding circuitry. It is generally best avoided by good spatial separation of leads, and proper isolation between them.

When attempting to quickly change the rate of current flow in a circuit, the change is counteracted by its **parasitic inductance** according to (equation 4.8).

$$\frac{di}{dt} = \frac{v}{L} \quad (4.8)$$

Where i is the current, v is the voltage causing the change in current and L is the inductance of the circuit. Inductance is strongly dependent on the lead area of a transmission line and counteract rapid changes in current transmission. To reduce parasitic inductance the leads should be kept as short and as wide as possible.

Naturally parasitic inductance causes a problem in high frequency current switching circuits, such as the one used in the laser current driver module in this project. Because of this it is important to utilize short, broad leads, and to have a good supply of decoupling capacitors to serve as energy storage between the pulses. The latter helps maintain the voltage in (equation 4.8).

Electromagnetic radiation can contribute to circuit noise as well. Magnetic fields are induced according to Maxwell's equations when a current is being drawn through a transmission line. These fields can couple into nearby leads, and induce undesired currents in other areas of the circuitry. Similarly, electric fields are induced and can be coupled whenever electric potentials are present.

Electromagnetic radiation is best countered by proper shielding of the wires or by using twisted pair (TP) solutions. The concept of twisted wires decreases interference because the loop area between the wires, which in turn determines the magnetic coupling into the signal, is reduced. TP wires in this project have been tested as a connection from the driver module to the laser.

Part III

Instrumentation and setup

The objective of the lab work in this project is to test various operation characteristics of the QCL, as well as produce a laboratory setup that can be used for IR spectroscopy, and measurements of gas concentrations in a sample. During testing with the QCL in this project, the laboratory setup in figure 4.14 has been used. It contains the driver module for producing the driving current of the correct magnitude and pulse length to the laser. In this project both the PCO 7120 driver module and the NEO design driver module have been subject to testing. However the NEO driver was used for all measurements concerning the actual QCL.

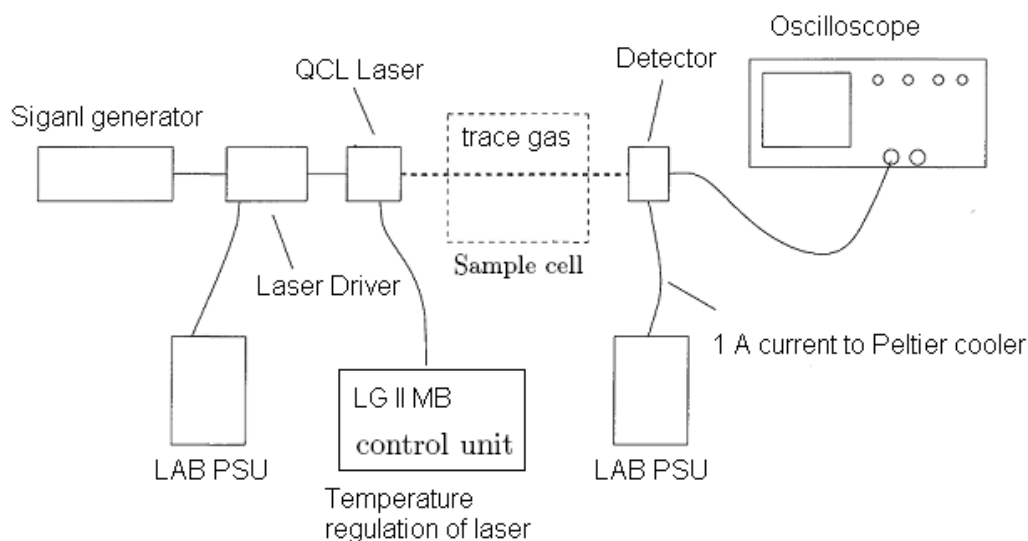


Figure 4.14: The laboratory setup with the driver module, its signal and DC inputs, the QCL with its LaserGas II temperature controller, the detector and its PSU for Peltier cooling, the oscilloscope, and a possible gas sample cell in the QCL ray path.

Upon receiving the QCL from NEO, it was mounted on a LaserGas II controller unit, near the back end of a 17 cm long, black aluminum tube. The tube has two main functions. Primarily it serves as protection for the QCL from its environments, secondly it holds a planoconvex, collimating CaF_2 lens at the front end. The lens itself is located approximately one focal length from the QCL, functioning as a collimator of the somewhat divergent beam from the laser, and enabling a higher beam intensity to reach the detector. Figure 4.15 shows the tube, and its cross section.

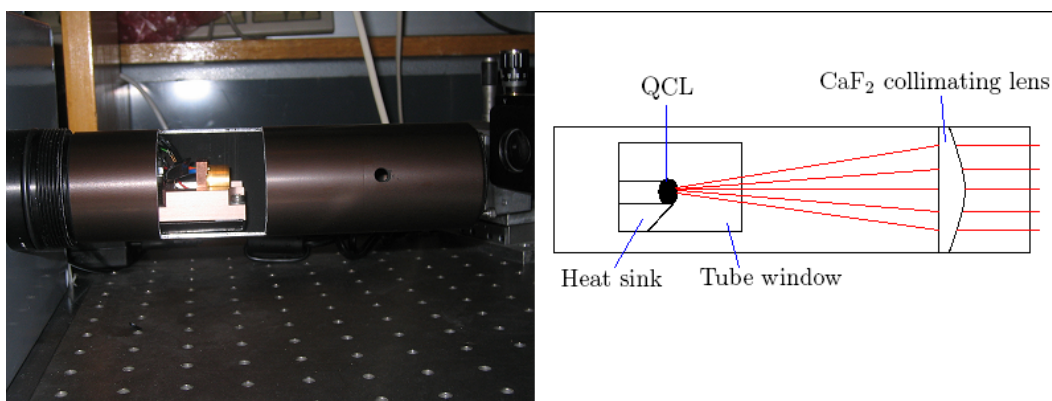


Figure 4.15: The actual tube (left), showing the QCL and a cut out window for accessibility. A cross section of the tube (right), showing the placement of the collimating lens.

5 Signal generation

During the course of this project two different QCL driver modules have been examined. The drivers need to be able to deliver high current pulses of pulse widths < 500 ns, and PRF of 1 kHz. Both of the drivers that have been tested require a readily generated input signal to set the output signal characteristics. The PCO 7120 driver module require an input of alternating 0-5 V with the same pulse width and PRF as the desired output signal. As it turns out, the NEO design driver module requires the same input characteristics as the PCO 7120 for operation with the component configuration that was ultimately used in testing of the laser.

The NEO design was also used for testing in my previous project [22], at the time using a Hewlett Packard 8004A pulse generator. This pulse generator however had strict limitations as to what voltage and pulse widths it could supply, as it was not configurable by the user. The main problem being the inability to adjust pulse widths. To avoid such restrictions during testing in this project, it was decided to generate the pulses using a National Instruments, PCI NI 5411, high speed arbitrary waveform generator card. This card was installed in a desktop computer, and programmed using LabView 8.

Labview in general utilizes a graphical programming language, called G , rather than a conventional Line by Line execution. Execution is in turn determined by the structure of a graphical block diagram, which implies that any node can execute as soon as all its input data become available. Since this might be the case for multiple nodes simultaneously, G is capable of parallel execution, that in turn can help speed up processes.

A LabView subroutine is called a virtual instrument (VI). Each VI has three components: a block diagram, a front panel and a connector pane. The latter may represent the VI as a subVI in block diagrams of calling VIs. LabView 8 contains a selection

of readily constructed VI templates that can be implemented or modified by the user. In this project the *arbitrary waveform generator* template was used as a basis for the signal generation.

Modifications to the arbitrary waveform generator template were done in the way that the *waveform array* was constructed. The waveform array was separated into a 0 V sequence, and a X V sequence. Each of the sequences were constructed using individual FOR-loops with a number of iterations specified by a *period* and a *pulse width* variable. The *X voltage* variable was set to 1 by default, and then adjusted by a *Gain* variable on the front panel.

The output signal could then be constructed using the above mentioned variables and a frequency variable, specifying the repetition speed of the entire waveform sequence. An image of the final VI front panel interface is showed in figure 5.16. The VI block diagram can be viewed in appendix J.

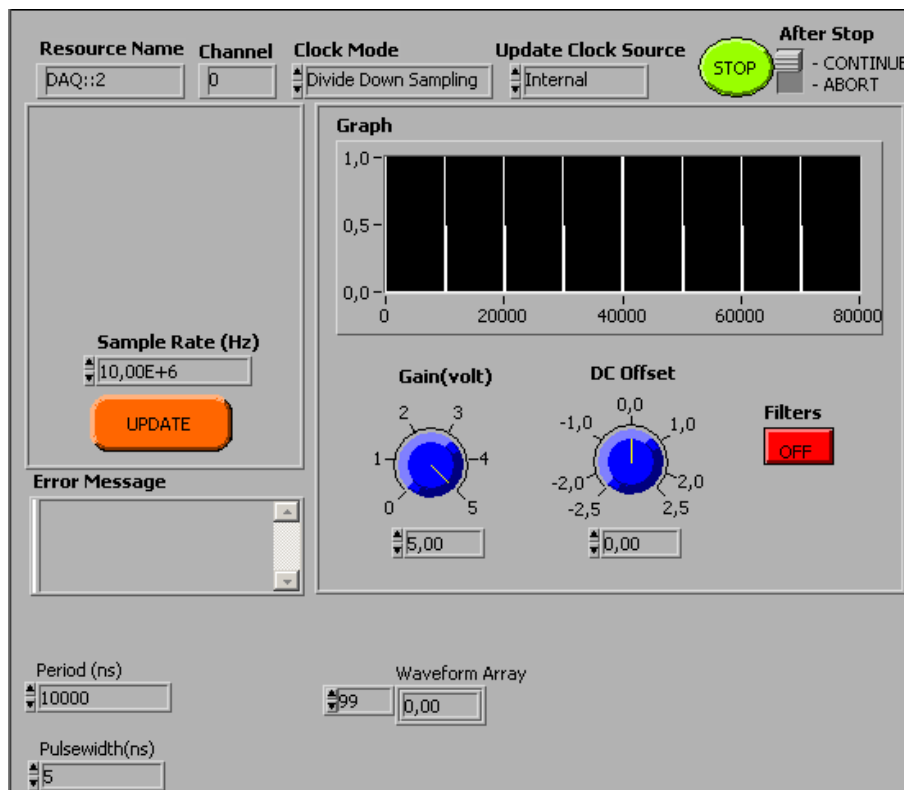


Figure 5.16: The LabView front panel interface used for generation of driver module input signals.

6 Lasergas II

The spectroscopy setup in this project is used in conjunction with NEO's LaserGas II SP monitor module. This is a system designed to monitor and control stationary, long term, industrial spectroscopy setups. The system can be used via a computer to measure and control the laser temperature and Peltier current. As well as provide information on gas concentration, line width, light transmission percentage, gas temperature and gas pressure. Such variables can be monitored and adjusted in the embedded gmw60 software. When all variables are set, the PC is no longer needed, as the monitor stores all variables in its internal memory. The LG II monitor and software can be viewed in figure 6.17.

In this project the the LaserGas II monitor has been used for temperature control of the laser alone. The temperature variable is set in the form of an internal thermistor resistance. Conversion from thermistor resistance to actual temperature, and vice versa, is done via a small script, named V2T2. In this project the QCL temperature has been maintained at 280 K.

More information on the LaserGas II SP monitor can be found in [16]. The mounting of the QCL with Peltier element and heat sink can be viewed in figure 6.18.

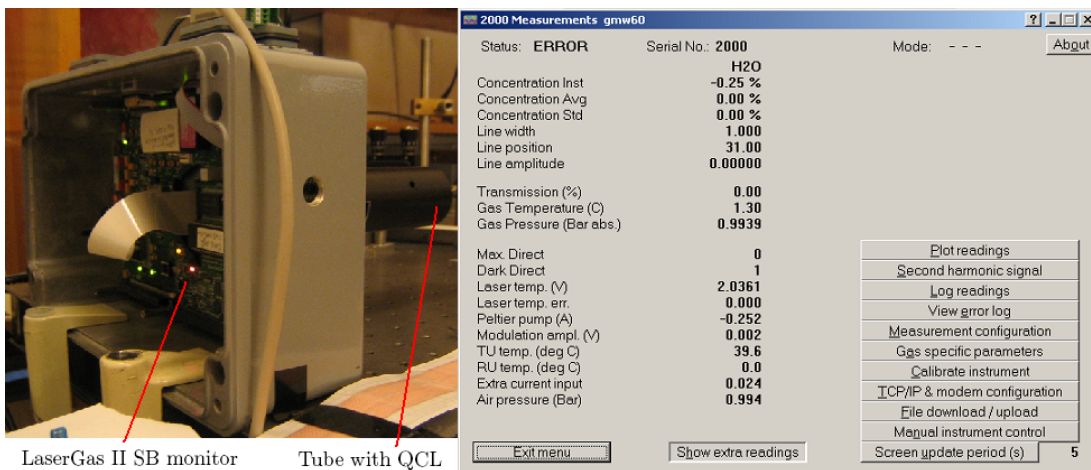


Figure 6.17: LaserGas II SB monitor (left) and the software interface for monitoring different variables (right).

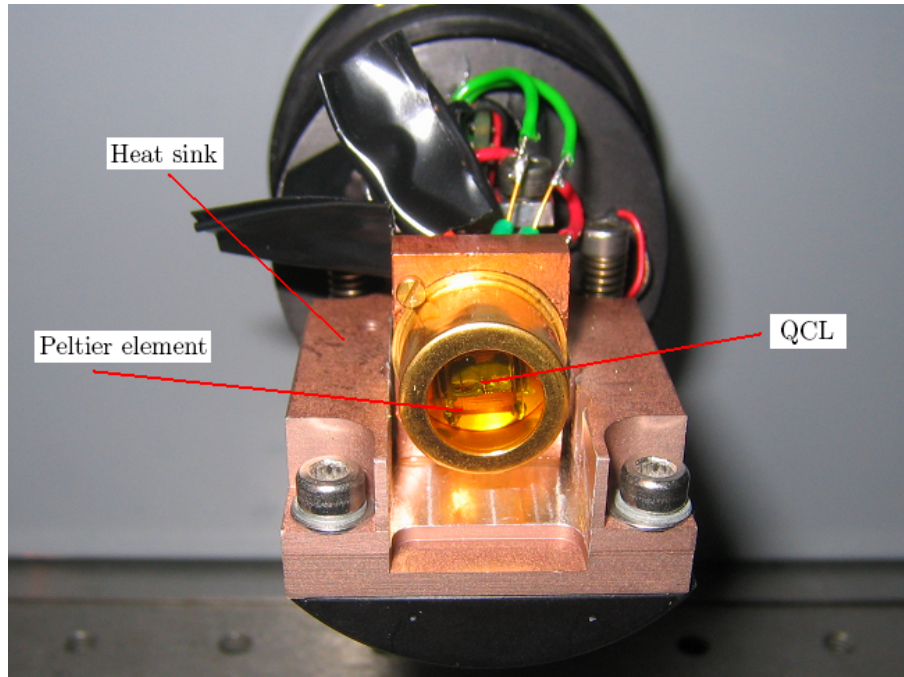


Figure 6.18: The laser mount showing the QCL, heat sink and Peltier element. Note that the aluminium tube has been removed.

7 The laser driver module

The initial task of this project has been to identify a suitable driver module for the QCL, or to improve the driver circuit constructed in my earlier project, [22], such that it meets the operation requirements. Pulsed operation of the QCL require short, accurate current pulses of a magnitude larger than the laser threshold current of 2.15 A, but lower than the laser maximum current value of 2.8 A. Ultimately, the driver module used for testing of the QCL would have to meet the following specifications (appendix A):

- Able to deliver current pulses of 1.5-2.8 A magnitude
- Pulse repetition frequency of 1 kHz
- Narrow pulse widths in the vicinity of 100 ns

During the course of this project, two different solutions have been considered and tested. One being the NEO circuit design from [22], and the other being the PCO 7120 laser diode driver module.

7.1 PCO 7120

As the driver module produced in my earlier project, [22], failed to achieve the required current pulse magnitude, NEO ordered a PCO 7120 pulsed laser diode driver module from Directed Energy Incorporated (DEI). This was done to ensure that the project could be continued, and so that this driver module could be used if the original design could not be altered to yield satisfactory results.

The PCO 7120 is designed to be quite versatile, supporting a wide range of output pulse widths, current amplitudes and pulse repetition frequencies. The complete list of specifications for the PCO 7120 can be found in appendix E. However the main challenge concerning application of the module in this project is that it is designed for current outputs from 5-50 A. To effectively operate the QCL, the driver needs to be able to supply tunable output current pulses in the range 1.5-2.8 A. It was decided that this can be solved in a laboratory setup by connecting the laser, or a laser equivalent, in parallel with a current limiting resistor.

The magnitude of the output current pulses for the PCO 7120 is controlled by a high voltage DC signal from 5-100 V (see figure 7.19). The module also utilizes a support power of 15 V. Basically it is desirable to get the current as low as possible, and therefore apply 5 V DC voltage to the driver.

With the minimum output of 5 A from the driver module, the following current limiting resistor value would deliver a current of 2.6 A to the laser, or laser equivalent:

$$R_{parallel} = \frac{V_{laser}}{5[A] - I_{laser}} = \frac{15[V]}{5[A] - 2.6[A]} = 6.25[\Omega] \quad (7.9)$$

However, to be able to gain the required tunability range, a lower $R_{parallel}$ value of 3.3 Ω should be chosen. The minimum value of I_{laser} can then be found from equation 7.9 to be 0.45 A. The current can then easily be tuned upwards by increasing the HV DC signal.

The PCO 7120 also needs a TTL gate input signal to dictate the PRF and the pulse width respectively. In this project the output from the NI 5411 card was used for this during testing. A picture of the PCO 7120 can be found in appendix E.

7.2 NEO design driver module

The driver circuit that was produced based on the NEO design did not yield a sufficiently high output during testing in [22]. However the circuit has been modified during the course of this project. Figure 7.20 depicts the initial, basic schematics of the NEO driver design. A slightly magnified image can be found in appendix D.

This implementation is constructed to receive a signal of low duty cycle, V_{in} , at magnitude of 0 and 5 V respectively. The input signal is then amplified through several BCV26 Darlington transistors, and supplied to the QCL at the driver output.

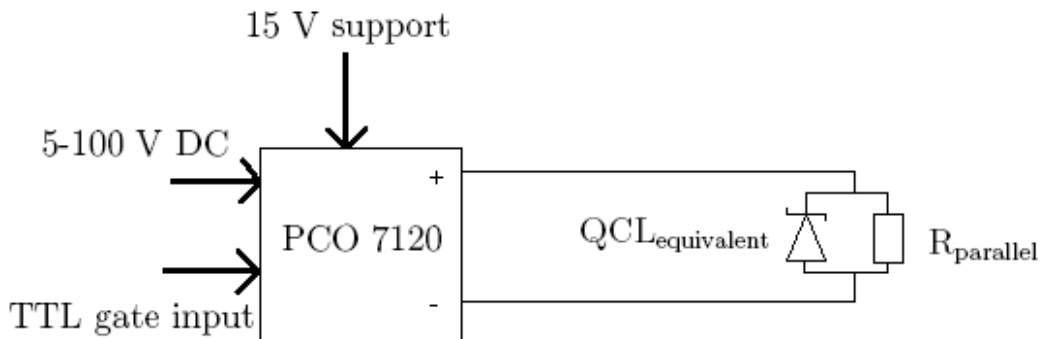


Figure 7.19: PCO 7120 with outputs, inputs and current limiting resistor.

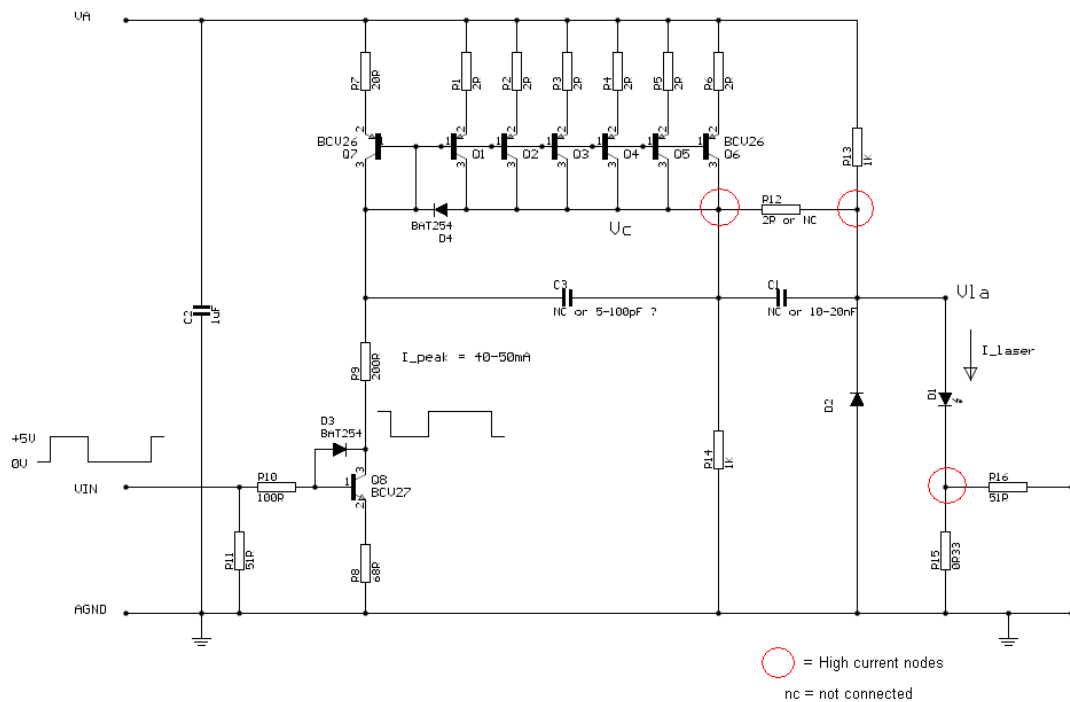


Figure 7.20: The initial driver design from NEO used in [22]

The QCL is represented by the diode, D_1 . To be able to adjust the amplification of the signal to yield the desired laser current, a supply voltage V_A is applied to the circuit as well.

The driver design provided by NEO is constructed to be used in two different implementations, referred to as case 1 and case 2. Case 1 is suitable to generate

average to long pulses, depending on the duty cycle of the V_{in} signal, while the case 2 configuration is designed to generate shorter pulses.

In both cases the driver design utilizes a current mirror technique to effectively amplify the input voltage. The current mirror in this design is triggered by the signal V_{in} sinking a current from the collector of transistor Q_7 . Sinking a current from the collector effectively generates a voltage difference, V_{BE} , between the base and the emitter of transistor Q_7 . This voltage will be the exact voltage that sustains the current I_C of Q_7 . Transistors Q_1 - Q_6 will have the same V_{BE} as Q_7 because they are all connected at the base and collector pins. Each transistor Q_1 - Q_6 , when matched to Q_7 , will then have a collector current of exactly 10x the collector current of Q_7 , because R_1 - R_6 is exactly 10x the value of R_7 . This current mirroring effect is independent of the gain coefficient β of each transistor, and is accurate as long as the individual temperature difference between the transistors is not too great, and as long as the transistors are not saturated. The inclusion of D_2 was done to prevent reverse voltages across the laser, as this would be devastating.

The case 1 set up utilizes a resistor R_{12} at the output of the current mirror. This will ensure that the output pulse width through the laser is the same as the pulse width of the V_{in} signal. Case 2 on the other hand has a capacitor C_1 connected at the output. This effectively shortens the pulse width delivered to the laser because C_1 only conducts during its charging phase (figure 7.21). In both cases the laser current is measured across a small resistor, R_{15} .

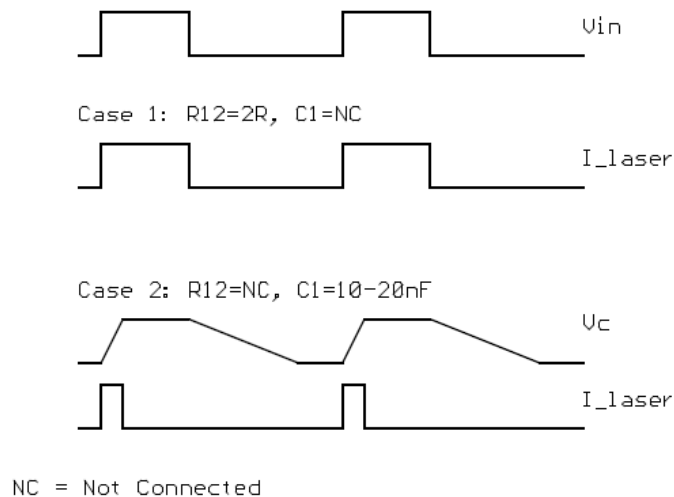


Figure 7.21: Sketch of I_{laser} vs. the voltage of the current mirror output.

Operating current for the QCL is 2.6 A (appendix A). The maximum I_c current for the BCV26 transistors used in the design is 500 mA. Because of this, 6 transistors are used in parallel to give a maximum possible output current of about 3 A.

The current delivered from the current mirror is given by:

$$I = 10 \cdot 6 \cdot I_{R_9} = 60 \cdot I_{R_9} \quad (7.10)$$

Where I_{R_9} is the current through resistor R_9 .

Resistors R_{11} and R_{16} are included to match the circuit to 50Ω coaxial cables for the input and output respectively.

7.2.1 Driver components

The circuit utilizes a variety of components. In the production of the circuit board only surface mounted components (SMD) have been used, so that the amount of drilling during production was limited to small via connectors. However, during testing some of the component values have been changed, and this was partially done by soldering non-SMD resistors directly on the circuit board. Initially most of the component changes were introduced to observe how the characteristics of the output pulses changed accordingly, but also to modify the circuit from case 1 to case 2 operation and vice versa.

Several of the components in the circuit also need to be able to lead high currents. Especially resistors R_1 - R_6 , and most of all R_{12} , needs to be of a size large enough to handle currents from 0.5-2.8 A. Because of this, 2512 sized resistors have been used in these cases as opposed to the smaller, more commonly used SMD0805 resistors. The mean power dissipated in the components should not be a problem when operating at duty cycles below 1 %.

All components and their values used in the two configurations are listed in (table 7.1). The table also holds information on the type of SMD component being used, and the packaging for the transistors and diodes. The last two entries are important when using software to design a PCB. Resistors R_1 - R_6 and R_{12} each have been split into 2 parallelly connected resistors to achieve the correct resistance.

The test plan provided in (table 7.2) shows which components that require to be changed in order to alternate between the case 1 and case 2 set up. It also shows the component values that were changed within each set up, to examine how the output pulse quality changed correspondingly.

During testing in my previous project the driver circuit was only able to reach an output magnitude of 1.58 A [22]. This output was reached using the case 1 configuration. Because the case 2 configuration provided generally less stable outputs, as well as output of lower magnitude, the case 1 configuration has been used for all further testing in this project. To increase the current output pulses to the value specified by the QCL data sheet, some troubleshooting and identification of noise contributions has been done, and the driver circuit has been modified to some extent.

Component	Value	Modified to	Component type	Package
R ₁₋₁	2.2 [Ω]	-	2512	-
R ₁₋₂	22 [Ω]	-	2512	-
R ₂₋₁	2.2 [Ω]	-	2512	-
R ₂₋₂	22 [Ω]	-	2512	-
R ₃₋₁	2.2 [Ω]	-	2512	-
R ₃₋₂	22 [Ω]	-	2512	-
R ₄₋₁	2.2 [Ω]	-	2512	-
R ₄₋₂	22 [Ω]	-	2512	-
R ₅₋₁	2.2 [Ω]	-	2512	-
R ₅₋₂	22 [Ω]	-	2512	-
R ₆₋₁	2.2 [Ω]	-	2512	-
R ₆₋₂	22 [Ω]	-	2512	-
R ₇	20 [Ω]	-	1206	-
R ₈	68 [Ω]	33	1206	-
R ₉	200 [Ω]	86	1206	-
R ₁₀	100 [Ω]	-	1206	-
R ₁₁	51 [Ω]	-	1206	-
R ₁₂₋₁	2.2 [Ω]	-	2512	-
R ₁₂₋₂	22 [Ω]	-	2512	-
R ₁₃	1 [k Ω]	-	1206	-
R ₁₄	1 [k Ω]	-	1206	-
R ₁₅	0.33 [Ω]	-	2512	-
R ₁₆	51 [Ω]	-	1206	-
Q ₁	-	-	BCV26	SOT-23
Q ₂	-	-	BCV26	SOT-23
Q ₃	-	-	BCV26	SOT-23
Q ₄	-	-	BCV26	SOT-23
Q ₅	-	-	BCV26	SOT-23
Q ₆	-	-	BCV26	SOT-23
Q ₇	-	-	BCV27	SOT-23
C ₁	nc or 10-20 [nF]	-	1206	-
C ₂	1 [μ F]	-	Tantal 35 V	B 3528
C ₃	nc or 5-100 [pF]	-	0805	-
D ₁ QCL equivalent	various	-	-	-
D ₂	-	-	BCG03-C24	DO214AC
D ₃	-	-	BAT254	SOD-110
D ₄	-	-	BAT254	SOD-110

Table 7.1: Component types and values used in 7.20. C is capacitor, R is resistor, Q represents a transistor and D represents a diode.

7.2.2 Modifications of the NEO design driver module

To improve on the results achieved by the NEO design during testing in [22], some modifications have been introduced to be able to use the design in testing with the QCL. Generally, it has been recognized that the layout of the PCB itself is less than ideal. One recognizable flaw, is that the leads on the PCB are generally constructed too long, and too thin. It is suspected that this is the cause of some major parasitic inductance throughout the circuit. This is especially of great concern when considering the high current nodes of the circuit (see figure 7.20), and the power rail where the supply voltage is applied. The relatively short pulse duration combined with a high

case 1:	Components					V _A	To test:			Testing order
	r12	d3	d4	c1[nF]	c3[pF]		V _{in} [V]	V _{out} [V]	I _{peak} [A]	
	2 ohm	nc	nc	nc	nc	15-25V	5	x	x	20
		c	c	nc	nc	15-25V	5	x	x	19

case 2:	r12	d3	d4	c1[nF]	c3[pF]	V _A	V _{in} [V]	V _{out} [V]	I _{peak} [A]	Testing order
		nc	nc	nc	10					
					5	15-25V	5	x	x	22
					20	15-25V	5	x	x	23
					40	15-25V	5	x	x	24
					80	15-25V	5	x	x	25
					100	15-25V	5	x	x	26
		nc	nc	15	nc	15-25V	5	x	x	27
					5	15-25V	5	x	x	28
					20	15-25V	5	x	x	29
					40	15-25V	5	x	x	30
					80	15-25V	5	x	x	31
					100	15-25V	5	x	x	32
		nc	nc	22	nc	15-25V	5	x	x	33
					5	15-25V	5	x	x	34
					20	15-25V	5	x	x	35
					40	15-25V	5	x	x	36
					80	15-25V	5	x	x	37
					100	15-25V	5	x	x	38
		c	c	10	nc	15-25V	5	x	x	1
					5	15-25V	5	x	x	2
					20	15-25V	5	x	x	3
					40	15-25V	5	x	x	4
					80	15-25V	5	x	x	5
					100	15-25V	5	x	x	6
		c	c	15	nc	15-25V	5	x	x	7
					5	15-25V	5	x	x	8
					20	15-25V	5	x	x	9
					40	15-25V	5	x	x	10
					80	15-25V	5	x	x	11
					100	15-25V	5	x	x	12
		c	c	22	nc	15-25V	5	x	x	13
					5	15-25V	5	x	x	14
					20	15-25V	5	x	x	15
					40	15-25V	5	x	x	16
					80	15-25V	5	x	x	17
					100	15-25V	5	x	x	18

Table 7.2: A table showing all the different circuit configurations of the NEO design. Each row in the table corresponds to one test configuration. *Testing order* states the order in which the configurations were tested. This is chosen for practical purposes, so that the least amount of components would be changed between each configuration. For each set up, V_{in} was constant and supplied by the signal generator. V_{out} is the voltage across R_{15} . I_{laser} is V_{out} divided by the value of R_{15} . V_A is the supply voltage ranging from 15-25 V. An X in the table signifies that this value was measured, or in the case of I_{laser} , calculated from V_{out} . NC means not connected, while C means connected. C is capacitor, R is resistor, Q represents a transistor and D represents a diode.

current sink, is causing the inductance of the PCB leads to limit the peak current value.

To rectify this problem, without the need of constructing a new PCB layout, a total of six decoupling capacitors have been applied between the power rail and ground. The capacitors serve as energy storage, and provide a much needed charge reserve when current is being sunk from the power rail. Ceramic capacitors of values from 400 nF to 1 μF were used in parallel, causing their combined capacitance to be added to the circuit. Figure 7.22 shows the added capacitors and the under dimensioned power rail and high current leads.

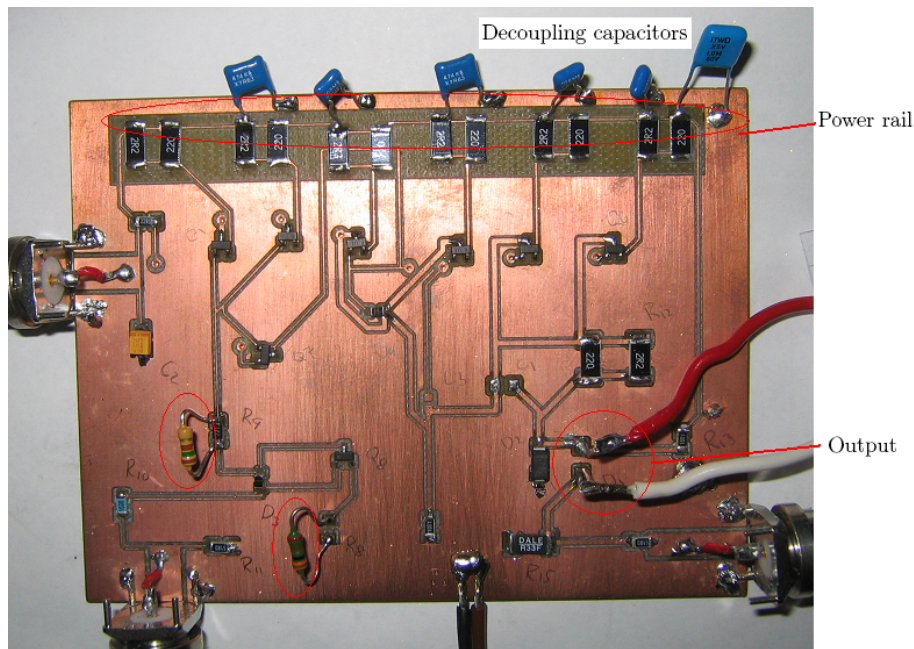


Figure 7.22: Addition of six ceramic capacitors between the power rail and ground. Also showing modification of R_8 and R_9

Another major problem that was revealed with the old circuitry was that transistor Q_8 was being saturated, effectively limiting the sinking current, I_{peak} in figure 7.20. To counteract this, the resistor values of R_8 and R_9 were decreased and increased respectively, according to (table 7.2). This modification can also be seen in figure 7.22.

The combination of the above modifications proved sufficient to increase the peak output current to the necessary level, thus eliminating the need to construct a new, generally improved layout. It was later shown during testing that the NEO design driver could produce current pulses of a magnitude of 0-2.8 A, with pulse widths of <500 ns, and short rise and fall times.

Part IV

Measurements and results

8 Testing of the driver modules with laser equivalent

Before connecting any current driver to the QCL it is of utmost importance that the characteristics and functionality of the driver have been well established beforehand. The laser has relatively small error margins concerning current pulses and none whatsoever concerning polarity of the connected signal. To ensure that the drivers functioned according to expectations, it has been vital to find a suitable laser equivalent that can be used for initial testing. The laser equivalent should have an I-V characteristic that closely resembles the actual QCL when a laser voltage, V_{laser} , is applied across its terminals. The I-V characteristic of the laser resembles that of a conventional diode, in the manner that it has extremely high resistance for low voltages below the lasing threshold. For voltages above the lasing threshold, a more linearly increasing I-V graph is observed.

To resemble this behavior a reverse biased zener diode has been used in series with a small resistor to create the laser equivalent (see figure 8.23). Matching the reverse breakdown voltage of the zener to the threshold of the original laser will then yield a resemblance to the desired effect. The value of the series resistor will represent the linear increase in the I-V graph after breakdown (see figure 8.24).

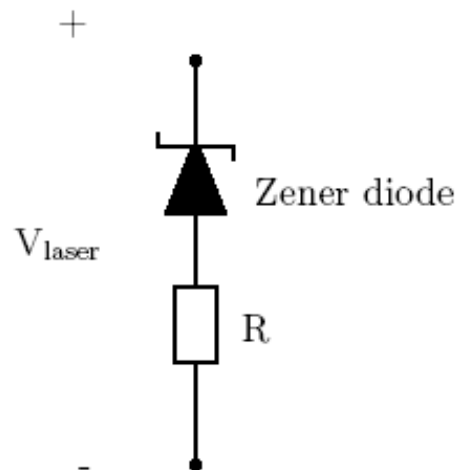


Figure 8.23: The QCL equivalent composed of a resistor in series with a reverse biased Zener diode.

In early tests of the NEO design driver module, such as in [22], a solitary BZG03C24

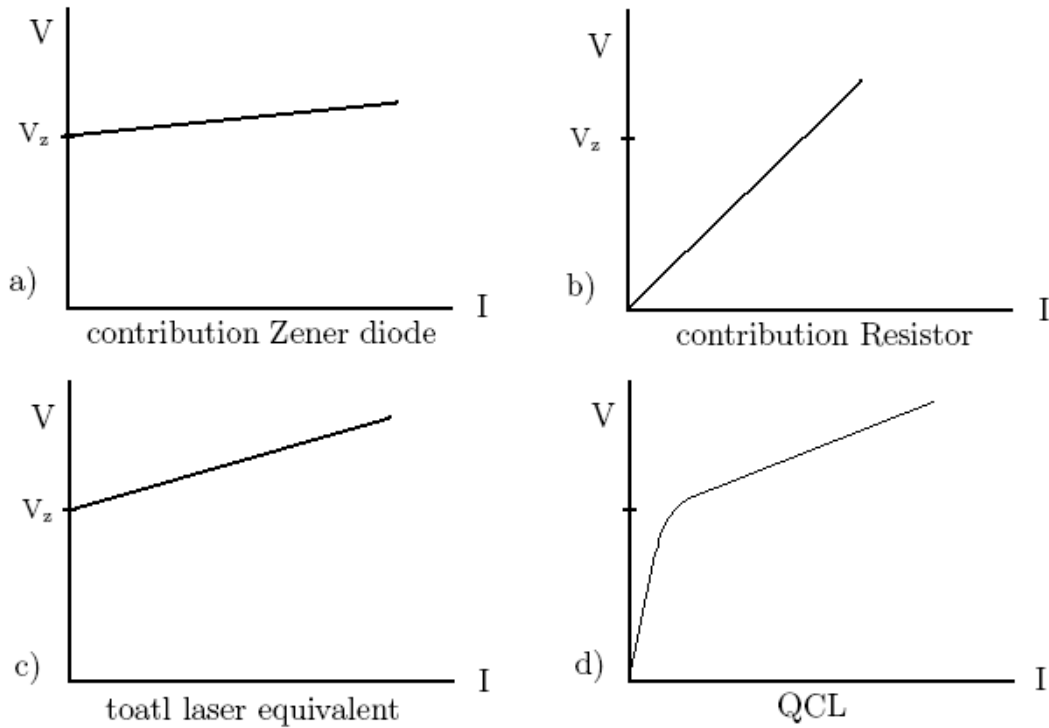


Figure 8.24: Theoretical outline of the laser equivalent I-V graphs. *b)* shows the contribution of the resistor, *a)* shows the contribution of the reverse biased Zener diode, and *c)* shows the superposition of the two, representing the total laser equivalent. *d)* shows the theoretical I-V characteristic of the QCL, which *c)* is supposed to resemble.

zener diode was used as a substitute for the QCL. This diode was *forward biased*, and was intended solely to test if the driver circuit could produce the necessary current magnitude. Likely this was a bad choice and may have contributed to the results of the initial testing being less than satisfactory [22].

Testing in this project has been done with a *reverse biased* zener, with zener voltage of 6.2 V, according to the above described setup. Data sheet for the zener diode can be found in appendix C. For the most part the serially connected resistor was skipped, due to the zener diode having a relatively large embedded resistance.

8.1 PCO 7120

Testing using the PCO 7120 as laser driver module has been somewhat limited. This is mainly because of the relative success of the testing done with the NEO driver. It was considered to be more educational to implement a self produced PCB in the testing of the laser. Also, it would be easier to alter or tweak the NEO design, following any possible unexpected functionalities, because of the genuinely better knowledge of the

circuit composition. The knowledge of the PCO 7120 was pretty much limited to the data sheet specifications (see appendix E).

The testing that was done with the PCO 7120 was mainly done to verify its functionality according to the product specifications (see appendix E), and to ensure that it could be easily implemented if the NEO design driver proved unusable.

Primarily the driver was connected to the necessary inputs, specified in figure 7.19, with the output connected solely across a $1\ \Omega$ resistor. A TTL input of 0-5 V, 500 ns pulse width, 1 kHz PRF was used. This was merely done to test that the driver module functioned according to expectations with a negligible load, solely used for current measurements. The resulting output graph can be viewed in figure 8.25. As the figure shows, the pulse shape is nice, with short rise and fall times. It has a duration of 500 ns as expected, and the magnitude was easily tuned by varying the high voltage DC input signal.



Figure 8.25: PCO 7120 output across a $1\ \Omega$ resistor. The voltage value is halved because of coax termination to the oscilloscope, making the real voltage 5 V. This corresponds to 5 A across a $1\ \Omega$ resistor.

8.2 NEO design

During testing of the different configurations of the NEO design (table 7.2), it has been established that the case 1 setup (figure 7.21) has been the only setup capable of producing a sufficiently high output current. This has effectively limited the relevant configurations to the ones labeled *testing order* 19 and 20 in table 7.2. Out of the two, the *testing order* 19 configuration was chosen for the remainder of the testing, because of the generally better results in my previous project [22].

Since it was decided that the NEO design driver was to be used for measurements with the QCL, it was thoroughly tested with the laser equivalent. Pulse quality and

magnitude was observed with the zener equivalent mounted in 3 different fashions. *Primarily* the zener was mounted directly on the PCB. This was done to eliminate loss or signal distortion arising from the transmission line from the PCB to the laser, so that any later addition of such noise could be more easily identified. *Secondly* the zener was mounted at the end of a 30 cm long twisted pair (TP) transmission line, consisting of two individually isolated copper wires that were twisted tightly around each other to form the transmission line. This was done to compare a classic TP, relatively long, wire solution to the PCB mount solution, and identify any degradation of signal quality. The *third* mounting configuration that was tested has the zener diode connected across the ends of two 30 cm long, 2.5 cm wide copper strips, with two isolating sheets of paper between them. In all further testing the signal input to the PCB from the NI 5411 has been 0-5 V, 500 ns, 1 kHz PRF pulses. The DC input has been used to tune the magnification of the pulses to the desired current value.

8.2.1 PCB mount

As mentioned the PCB zener diode mount was done to acquire output pulse images with the least amount of added transmission line noise. The placing of the zener diode can be viewed in figure 8.26.

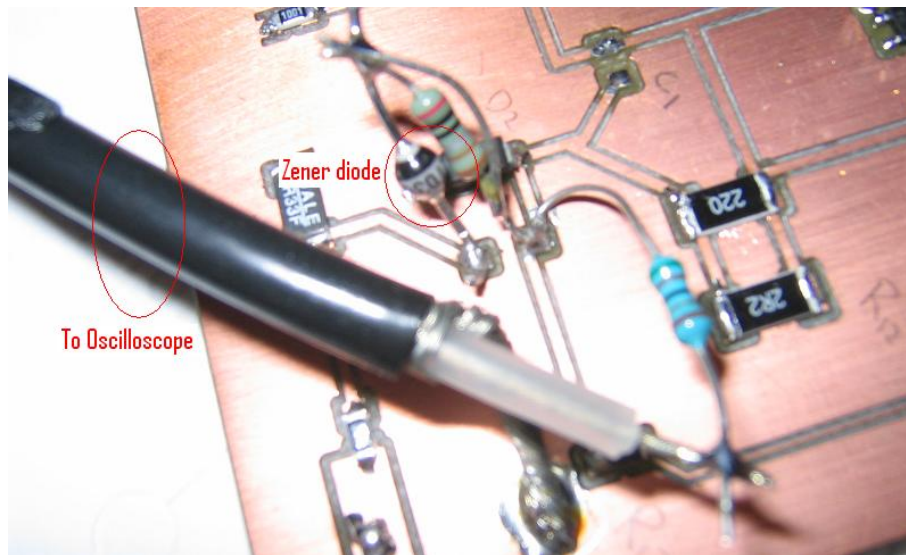


Figure 8.26: Zener diode mounted directly on PCB. Also showing coax cable to oscilloscope, and 50 Ω terminating resistor (blue)

The resulting oscilloscope image of the PCB mounted laser equivalent configuration can be viewed in figure 8.27. This image shows the voltage measured across the reference 0.33 Ω resistor, R_{15} in the NEO design circuit (see 7.20). As previously mentioned, this voltage is only half of the actual voltage because of the 50 Ω termination resistor. Bearing this in mind, the voltage on the oscilloscope must be multiplied by

two, and then divided by 0.33 to attain the appropriate current magnitude. The latter of course being of great importance when driving the QCL. In figure 8.27 the voltage is controlled by the DC supply voltage of the PCB to equal 396 mV across the output reference resistor, R_{15} . This in turn corresponds to 2.4 A of current through the zener diode.

It is evident that the pulse shape is satisfactory, with very short rise and fall times. There is almost no pulse broadening, at least above 1.2 A, and the general pulse width is close to 500 ns. There were no problems in tuning the magnification of the pulses in the desired range, up to about 2.8 A. For oscilloscope pictures of some other peak current values, refer to appendix F.

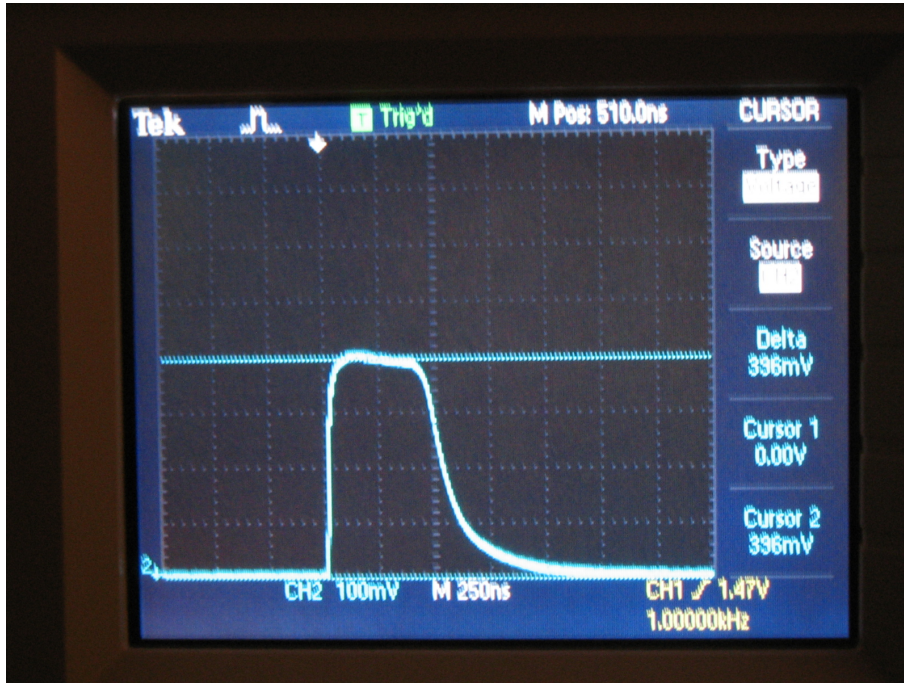


Figure 8.27: Output from PCB with laser equivalent zener diode mounted on PCB. Peak voltage of 396 mV corresponding to 2.4 A current magnitude. Pulse width of 500 ns.

8.2.2 Twisted pair mount

A twisted pair transmission line approach was used as a way to easily implement a connection from the PCB to the laser, while offering less of a noise addition compared to a non TP solution. Figure 8.28 shows the TP wires connected to the PCB and the zener diode. The resulting oscilloscope image of the TP mounted laser equivalent configuration can be viewed in figure 8.29.

With this configuration it is easily observed that the addition of the twisted copper wires drastically degrades the pulse quality. Bearing in mind that the inputs to the

PCB are the same, we can see that the rise time of the pulse are greatly increased. Although it is not crippling at this pulse width it is likely to be a much bigger problem if an attempt to further decrease the pulse width is made. The increased rise time of the pulse is caused by the added parasitic inductance in the TP transmission line, ultimately making the TP wires less ideal than the direct PCB mount when operating at lower pulse widths. Of course this was to be expected as well. For oscilloscope pictures of some other peak current values, refer to appendix F.

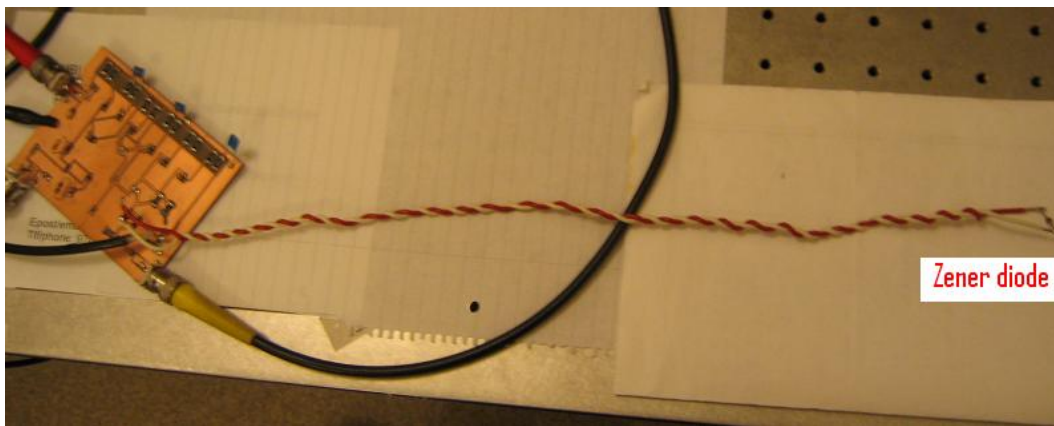


Figure 8.28: Zener diode mounted at the end of 30 cm long twisted copper wires.

8.2.3 Copper strip mount

The implementation of wide copper strips as a transmission line is theoretically going to decrease the amount of parasitic inductance added to the circuit. Generally the strips offer a much larger lead area, which should reduce the added noise component. However the strips pose a greater threat in the lack of electromagnetic shielding, and care should be taken not to short circuit the leads to any surrounding surfaces. In figure 8.30 the strips have been separated with 2 sheets of paper, and clear plastic tape has been applied to offer isolation.

The resulting oscilloscope image of the copper strip mounted laser equivalent configuration can be viewed in figure 8.31. It is observed that the pulse rise time has been greatly reduced compared to the previous image from the TP mounting. The improved rise time of the pulse, the lack of significant pulse broadening, and the ability to still tune the current amplification in the desired range, lead to this configuration being used in all testing with the actual QCL. For oscilloscope pictures of some other peak current values, refer to appendix F.

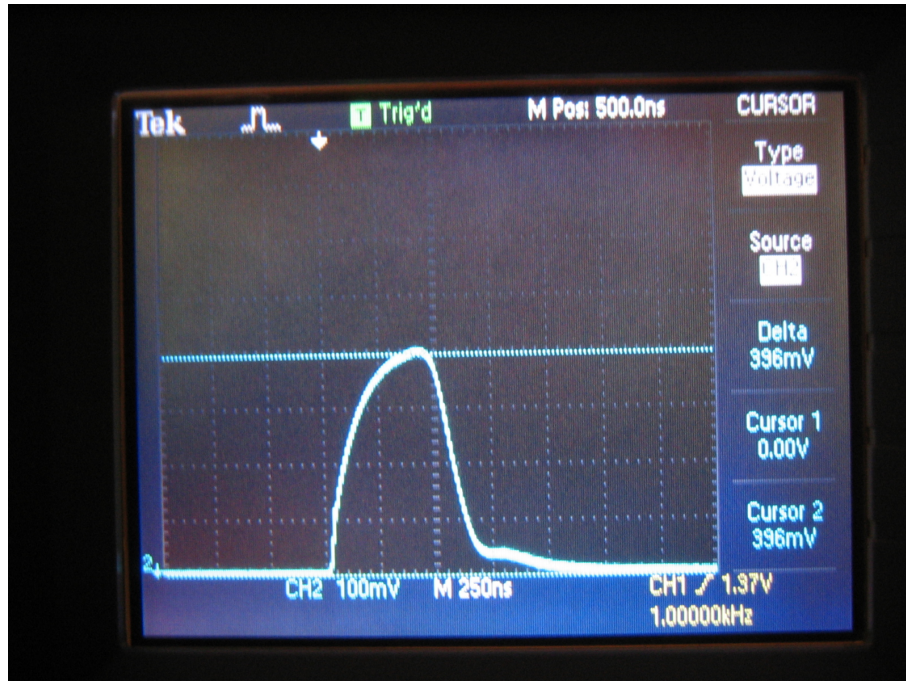


Figure 8.29: Output from PCB with laser equivalent zener diode mounted at the end of 30 cm long TP copper wires. Peak voltage of 396 mV corresponding to 2.4 A current magnitude. Pulse width of 500 ns.



Figure 8.30: Zener diode mounted at the end of two 30 cm long, 2.5 cm wide copper strips. Paper isolation in between. The bottom (positive) strip is not showing.

9 Testing with the QCL

9.1 Verification of polarity

Upon beginning the testing with the actual QCL, a few things were considered. The testing with the zener equivalent showed that the NEO driver design was working

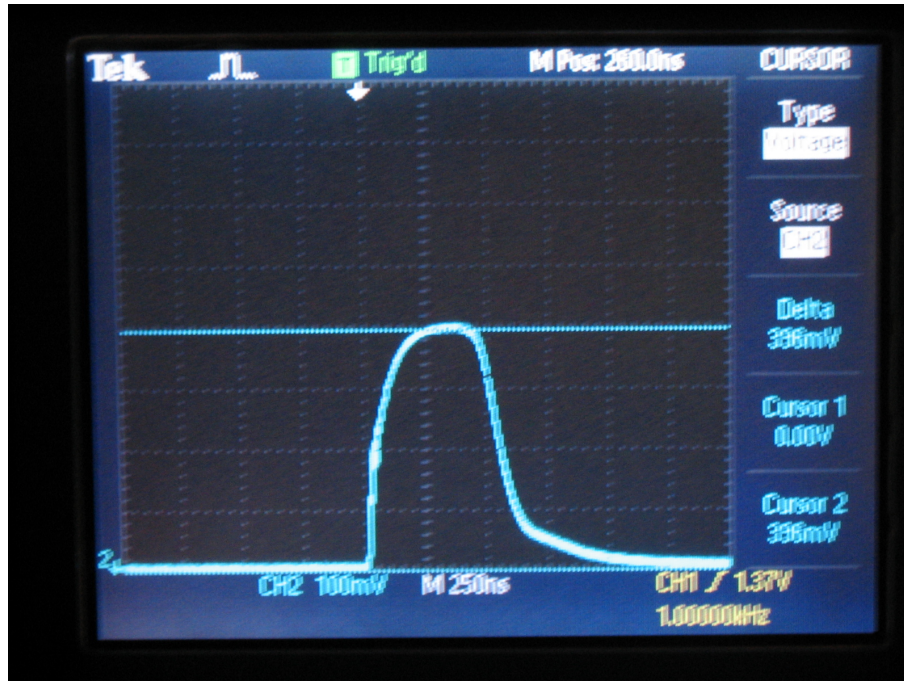


Figure 8.31: Output from PCB with laser equivalent zener diode mounted at the end of 30 cm long, 2.5 cm wide copper strips. Peak voltage of 396 mV corresponding to 2.4 A current magnitude. Pulse width of 500 ns.

satisfactory and should be able to produce good quality current pulses with a tunability range from 0-2.8 A. However the polarity of the signal when connected to the QCL should be verified. The pin configuration of the QCL mounting pad can be found from its data sheet (appendix A), but bearing in mind that even small reverse voltages across the laser terminals could destroy the laser, it was decided to implement a safety precaution.

As can be seen in figure 8.24, the I-V graph of the zener diode equivalent will have a larger derivative for low voltages than the QCL. Because of this the QCL and the zener diode were initially mounted in parallel. Then some low voltages were applied across the output. If the QCL was mounted with the wrong polarity, the resulting I-V graph for low voltages would follow that measured using only the zener diode. The reason for this is that the QCL would lead no current in this case. However when the QCL was mounted with the correct polarity, the measured I-V graph would deviate slightly, as the QCL would be leading a low current. More specifically the measured I-V graph should have a lesser derivative than that of the zener diode alone.

The results can be viewed in figure 9.32, and clearly shows the QCL/zener combination graph being less steep for low voltage values. It is also evident that the voltage of the combined QCL/zener configuration does not exceed the voltage of the Zener configuration. This is because the zener diode has lower resistance for voltages above

6.2 V.

Having ensured that the laser was mounted with the correct polarity, the zener diode was removed for all further testing.

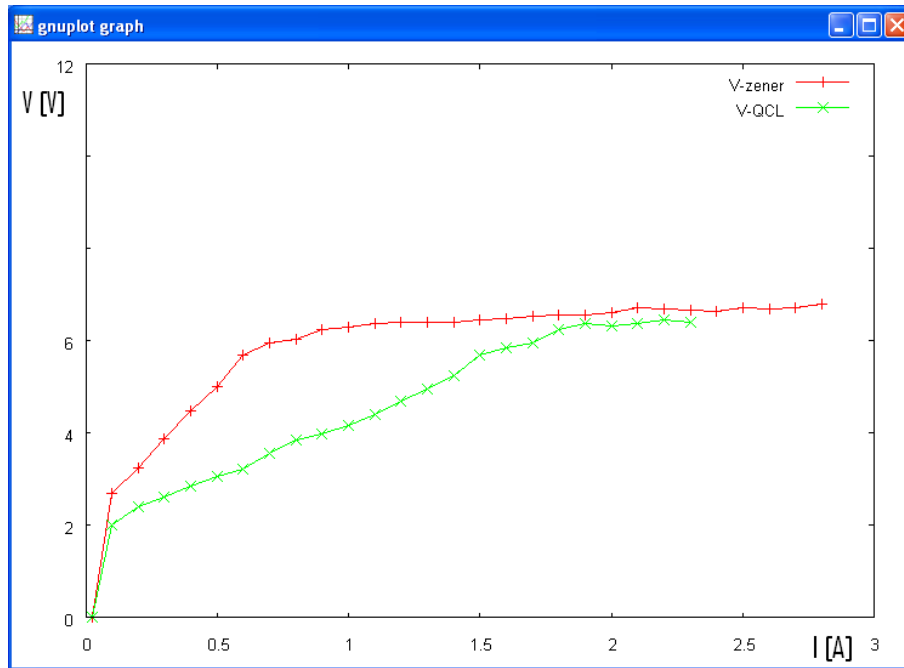


Figure 9.32: I-V characteristics measured for the zener diode alone (red), and the QCL and zener diode in parallel (green). The zener breakdown at 6.2 V is clearly visible.

For all consecutive measurements with the laser, the pulse quality and magnitude were monitored on the oscilloscope. This was necessary to ensure that the pulse magnitude did not exceed the I_{\max} of 2.8 A. An image of the pulse quality that was achieved and used in all subsequent testing can be viewed in figure 9.33.

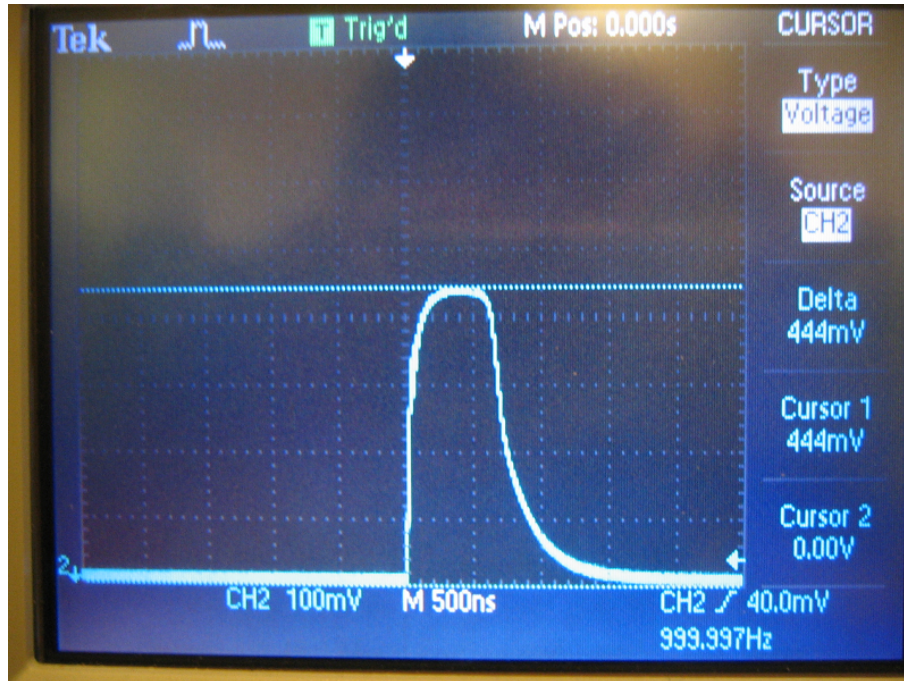


Figure 9.33: Reference voltage corresponding to a peak current magnitude of 2.7 A. Voltage measured across the reference resistor, R_{15} in the NEO design driver circuit.

9.2 Producing the I-V characteristics of the QCL

Measurements of the QCL's I-V characteristics were also done before introducing the detector in the setup. It was done to verify that the resulting graphs were consistent with the theoretical outline described in figure 8.24. A satisfying I-V graph also provided some confidence towards the fact that the QCL was working properly before attempting to align the beam with the detector.

The procedure consisted of measuring the voltage across the reference resistor, while increasing the peak current in 0.1 A increments. The resulting graph can be viewed in figure 9.34.

9.3 Conducting measurements with the Vigo detector

The detector from Vigo has a responsivity of $1.4 \left[\frac{\text{A}}{\text{W}} \right]$ at a wavelength of $7.42 \mu\text{m}$, measured at 230 K (see appendix B). This wavelength is at the top of its responsivity curve, making it propitious for use in this project. The operating temperature of the detector is controlled by a Peltier current supplied from a lab PSU. According to the data sheet, the maximal Peltier current is 1.4 A, while the optimal current is listed as 1.2 A. A Peltier current of 1.2 A in our laboratory environment was able to cool the detector to a temperature of 232 K. This has been the operating temperature for all

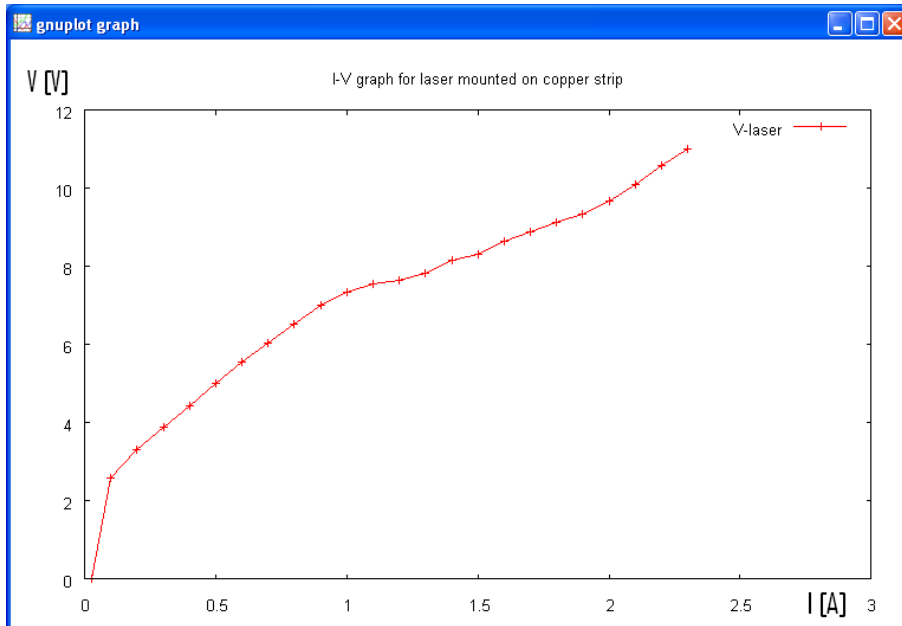


Figure 9.34: I-V characteristics of the QCL mounted at the end of 30 cm long, 2.5 cm wide copper strips. Voltage measured at intervals of 0.1 A. The data are plotted in GNUplot.

consecutive testing. Temperature monitoring of the detector was done by constantly measuring the resistance of the built-in thermistor.

To ensure that the Peltier current would not get too high, which in turn could destroy the Peltier element, a simple procedure was followed. Upon switching on the PSU, but before connecting it to the detector, the voltage and current were both turned to 0. Then the voltage was turned quite high, and the current was set to the appropriate value using an oscilloscope. Subsequently the voltage was turned down again until the current started dropping. This effectively ensured that the current could not go above the set limit, even with instability in the PSU.

With the detector operating at the lowest possible temperature, a simple test of detector functionality was conducted. Taking advantage of the fact that the detector operates in the IR frequency region, it should have the ability to detect heat waves. Following this, a soldering iron, heated to 673 K, was brought into the vicinity of the detector surface. This did indeed produce a detector current, and thus the detector was proved to be functional. Subsequently the detector was placed within the beam path of the QCL.

To be able to single out the detection of the short pulses from the laser, the detector was connected to a separate oscilloscope, being triggered by the TTL input signal to the driver module. This was necessary because of the relatively short pulse durations compared to low pulse repetition frequency. Also, to more easily be able to adjust the accurate position of the detector, it was placed on a 3 dimensional coordinate table

mount.

During attempts to align the detector for the best possible signal output, a $50\ \Omega$ shunt resistor was inserted to suppress noise, and improve the quality of the detected signal.

Producing satisfying results with the detector has indeed proved difficult during testing. The process of obtaining a good alignment of the laser beam is necessarily subject to a trial and error approach, and made more complicated due to the invisibility of the laser beam.

An effect on the detector has been identified, but it is well below what should be expected if the laser was working according to expectations, and if the beam was properly aligned. Because of the extremely low signal value that has been produced by the detector, it has been difficult to isolate, or at least distinguish, from small, added noise components. The results from the best obtained beam detection can be viewed in figure 9.35.

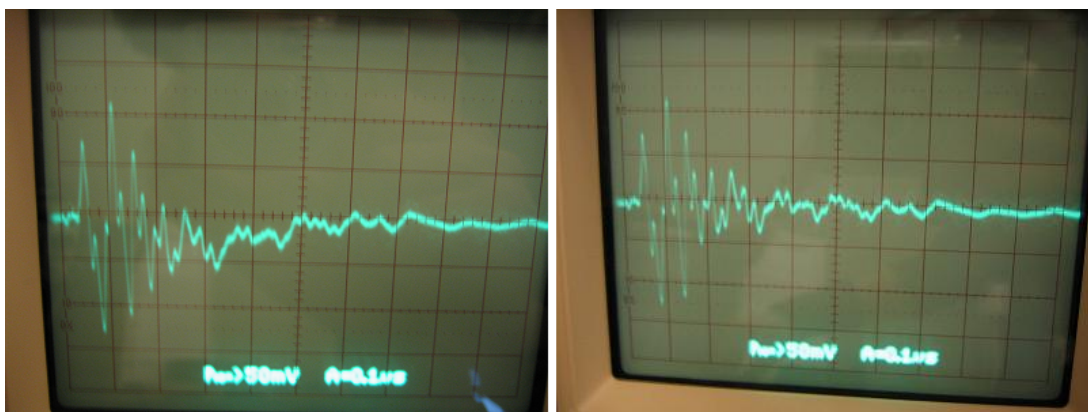


Figure 9.35: Pictures showing the comparison of detected laser signal (left), and object blocking the laser path (right). Resolution is 100 ns per square on the x-axis, and 5 mV per square on y-axis.

The reason for the negative voltage contribution of the laser beam is that the polarity of the connection to the oscilloscope is reversed. Also the oscilloscope shows a 10x y-axis magnification, this meaning that the resolution is 5 mV per square rather than 50 mV.

From the image it is seen that the laser beam only contributes to about 3 mV of output voltage across the $50\ \Omega$ shunt resistor. Removal of the resistor has only made the noise component greater, without adding noticeably to the results. The inability to detect a larger signal could arise from poor alignment of the beam, poor output from the QCL, or problems with the detector itself.

It is notable however, that the added noise component is far greater in the first 200 ns of the pulse, making it possible that the output could be slightly higher during this period.

Several approaches have been made to increase the detected signal:

- Measurements using several different oscilloscopes, eliminating possible defects or malfunctions
- Removal of the 50 Ω shunt resistor on the detector signal. It provided no better detection results, but added some minor noise components.
- Complete inspection of all ground planes in the circuitry. Shorter, broader leads were introduced in most ground connections. Measurements on ground planes showed some fluctuating potential during pulse duration (see appendix I). When new leads with lower inductance were introduced, the noise components on the signal was somewhat reduced. The detected signal strength however did not increase noticeably.
- Most of the cables in the entire setup was exchanged with shorter counterparts. They were also separated as much as possible to reduce electromagnetic radiation.
- Removal of all possibly interfering electronic apparatus in the laboratory environment.
- Detector placement was changed in the x-y plane to attempt better alignment. The distance from the detector to the QCL was also altered from a few millimeters to several decimeters.
- Pulse widths were altered from 500 ns to 1.5 μ s

Ultimately, none of these measurements provided any better detection results. However, one notable discovery was made when attempting to align the detector in the x-y plane, perpendicular to the beam path. It seemed that the best detection results were achieved when the alignment was slightly off center, in the x-y plane. Figure 9.36 depicts this phenomenon.

It was thought that the phenomenon in figure 9.36 could arise due to reflections of laser light off the tube walls, or failure to transmit light along the center beam path. The latter could be explained if the CaF_2 lens had poor transmission along the center path. To examine this problem further, some alterations were made.

- It was attempted to remove the aluminum tube, and place the detector close to the QCL without the use of a collimating lens. This did not improve noticeably on the detection, however the placement of the heat sink of the laser limited the minimum distance to about 1 cm.
- Ultimately, an identical CaF_2 lens was placed on a holder between the QCL and the detector, with the original lens and aluminum tube removed. This was done to be able to better adjust the distance from the laser to the collimating lens, to eliminate reflections off the tube walls, and also to eliminate any defects in the original lens.

The removal of the tube, and exchange of the collimating lens did not improve noticeably on the detected signal strength. It seemed however, that the removal of the

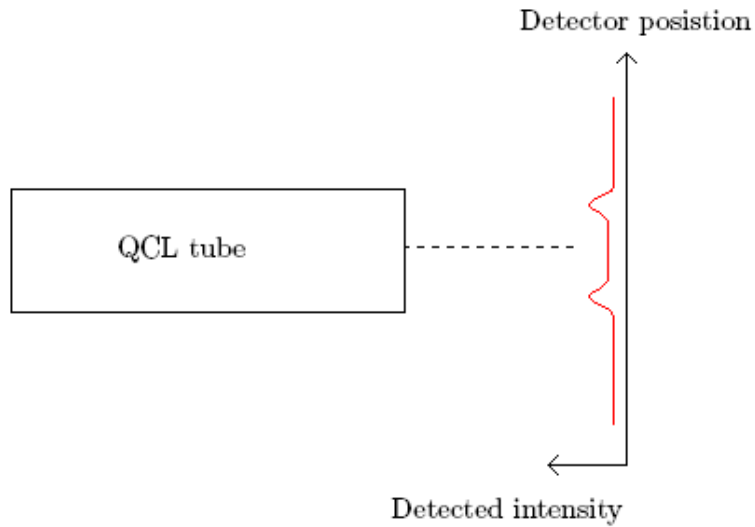


Figure 9.36: Top view of the QCL tube and detector placement. Showing a slightly better detection with the detector being a small distance off the center alignment. Distance from tube to detector plate is kept fixed.

tube did remove the effect in figure 9.36. This gives ground to believe that the phenomenon could have been caused by reflections off the tube, but offering no apparent solution as to why such a low intensity was detected.

Part V

Discussion of results

The measurements conducted in this project have in general yielded results according to expectations. The characterization of output power from the laser however proved more difficult than anticipated.

Primarily the modifications of the NEO driver module have proved successful. However the general layout of the PCB still has flaws, and can be further optimized. In retrospect, the PCB layout would ideally have been redone, in a manner that made it less susceptible to coupling noise. The layout should be concentrated onto a smaller PCB area, making the leads wider and shorter in the process. This is especially true for the high current leading nodes near the output, and for the power rail. As described in [22] the circuit was unable to produce sufficiently high current pulses in its original form. However it has been shown that the introduction of several large decoupling capacitors, and alteration of bottle neck resistor values were able to reduce the noise components to the degree that the output specifications could be met. Especially changing the value of resistors R_8 and R_9 was able to bring transistor Q_8 out of saturation, effectively increasing the programming current of the current mirror. When both the current pulse magnitude, its tunability, and the rise/fall times of the output were made satisfactory, it was decided not to spend time designing and printing a new circuit board.

Results made with the PCO 7120 driver module were few as it was abandoned during initial testing, due to the positive results of the NEO driver tests. It did however produce good quality pulses with easy tuning of pulse magnitude. There should not be any difficulties in incorporating the PCO 7120 into future testing with the QCL, bearing in mind that the current limiting resistor is necessary to reduce the current below the specified limit of 5 A.

The utilization of laser equivalent testing was done to avoid unnecessary damage to the QCL. It provided a way to characterize the functionality of the driver module and connected transmission lines, without exposing the laser to undesired voltages or noise components. The tests revealed that the choice of the BZT03C6V2 zener diode as laser equivalent was a good choice. Its I-V characteristic proved to be quite similar to that of the actual QCL. Because of the constant monitoring of the current pulses during QCL testing, and the ability to tune current magnitude using the DC driver input, it was not necessary for the I-V graphs of the equivalent and the laser to match exactly.

During testing of the two different types of transmission lines from the driver module to the laser, the low inductance copper strip proved superior to the twisted wire solution. This was expected because of the large lead area that the copper strip provides. The generally lower inductance of the copper strip can be viewed in the noticeably shorter rise time of the pulses, ultimately making it possible to generate much shorter

pulses with this solution. The similarity between the pulses observed with the copper strip mount and the mounting directly on the PCB gave no apparent reason to attempt other transmission line solutions.

Generation of the QCL I-V graph was done by incrementing the current pulse magnitude in intervals of 0.1 A, and measuring the corresponding laser voltage. The results were according to expectations, although initially there was little knowledge of the actual I-V characteristic that the laser should follow. The derivative of the curve should be higher for low current values, and progress to be lower as the QCL approaches its threshold. This was verified by the results.

Testing with the Vigo detector proved to be more difficult than anticipated. It was expected to be challenging to achieve a good alignment between the laser beam and the detector chip. However, extensive adjustment of the detector position did not yield good results. The magnitude of voltage detected was <5 mV across a 50Ω shunt resistor. Given the expected output power of the laser, this should be in the 100-200 mV area with a proper alignment. Several attempts were made to increase the detected signal, none of which proved successful. Ultimately the detector was placed 1 cm from the QCL with the collimating CaF_2 lens removed. This approach should ideally have eliminated problems caused by the lens, the aluminum tube and by alignment. The removal of the collimating lens would contribute to a reduced detection by itself, as the beam is somewhat divergent when emitted from the laser. However, if the detector and QCL were functioning according to expectations, the detected signal should still be higher.

As this project is concluded, the problem causing the low detected signal is not resolved. It is suspected that either the detector or the laser is not working according to expectations. If they are, the only remaining factor is the alignment of the laser beam. The alignment has proved difficult to verify because of the inability to detect a good signal, and the lack of means to visually confirm the beam.

Part VI

Conclusions

Norsk Elektrooptikk wishes to implement their Nanoplus G2102/DFB2/5-12 QCL in trace gas detection spectroscopy. During this project it has been attempted to produce a laboratory setup for basic trace gas spectroscopy using the Nanoplus Quantum Cascade Laser, a LaserGas II SP monitor, a PVI-2TE-8 Vigo photovoltaic detector, and a self constructed laser driver module. Measurements of the laser I-V characteristics have been conducted, and it has been attempted to achieve an accurate detection of the laser output power.

Initially the driver module has been modified from its original design to be able to generate the desired 2.8 A, <500 ns pulse width, 1 kHz PRF pulses needed to operate the laser. This was achieved with satisfying results by introducing several large ceramic decoupling capacitors between the power rail and ground, and by changing the resistor values affiliated with the generation of the program current for the current mirror in the design.

Generation of the TTL signal input to the driver module has been changed from a Hewlett Packard 8004A pulse generator to a PCI NI 5411 high speed arbitrary waveform generator card. Control of the NI 5411 has been done through a modified LabView 8 VI template. This has offered a better versatility in creation of the pulses and ultimately of the current pulses supplied to the laser.

Two different transmission line solution have been studied for connecting the driver module to the QCL. A 2.5 cm wide, 30 cm long copper strip implementation was chosen because of its low contribution to the circuit inductance, and the generally lower rise times of the pulses compared to the twisted wire solution. With this solution the driver module now delivers pulses of the required magnitude, good tunability and a nice pulse shape with little broadening effects. It should not prove a problem to reduce the pulse widths further in future experiments.

An I-V characteristic for the QCL has been produced by incrementing the laser current and measuring the corresponding laser voltage. The graph produced verifies the expected curvature, showing a steep climb for low current values, with gradually lower resistance and a less steep increase for current values approaching the lasing threshold.

Measurements of the laser output power using the Vigo detector has proved difficult. The maximum voltage detected across the 50 Ω shunt resistor has been 3 mV. This is less than should be expected. The results are likely contributed to poor alignment of the laser beam or unexpected functionality of the laser or the detector. x, y or z-axis movement of the detector, as well as removing or exchanging the collimating lens, has proved to yield little effect.

Part VII

Outlook and future work

The process of characterizing the P-I behavior of the QCL in this project was cut short due to the inability to produce a significant detector signal. It is evident that the detected signal should be several 100 mV higher than what was recorded if all components were functioning according to expectations and a proper alignment was achieved.

This leaves a certain amount of future work if the QCL is to be used in spectroscopy applications with the current setup. Arguably there can be three reasons for the poor detection:

- The QCL is not producing an output according to expectations
- The detector is not functioning properly at the given wavelength.
- Poor alignment between the laser beam and the detector.

To continue with experiments each of these three possibilities will have to be examined. Generally it is most likely that the beam was not properly aligned. In the current setup it was not possible to get a signal that was good enough to further help improve the alignment. Because of the small detector voltages it was difficult to distinguish the noise components, although small, from the actual signal.

If a good alignment could be achieved, and in turn produced a better detector signal, it would be possible to go forward with spectroscopic measurements and thorough characterization of the QCL using the current setup.


References

- [1] Alexander Bernt. *Assembly and implementation of a DFB QCL emitting 5.4 um into a TDLAS Laser Gas Monitor*. Lehrstuhl für Thermodynamik, 2005.
- [2] Douglas Brooks. *Transmission line terminations*. UltraCad design, Inc., <http://www.ultracad.com>.
- [3] ATIS committee T1A1. *ATIS Telecom Glossary*. American National Standard, <http://www.atis.org/tg2k>, 2000.
- [4] Dung Do Dang. *Wavelength modulation spectroscopy with single modus optical fiber*. IET NTNU, 2005.
- [5] Claire Gmachl; Federico Capasso; et al. *Recent progress in quantum cascade lasers and applications*. Bell Laboratories, Lucent Technologies, 600 Mountain Avenue, Murray Hill, NJ 07974, USA, 2001.
- [6] Daniel Hofstetter; et al. *High-temperature operation of distributed feedback quantum-cascade lasers at 5.3 mm*. Applied Physics Letters, Volume 78, Number 4, 2001.
- [7] I. Linnerud; P. Kaspersen; et al. *Gasmonitoring in the process industry using diode laser spectroscopy*. Applied Physics, B 67, 1998.
- [8] J. Faist; F. Capasso; et al. *Quantum design of QC-laser*. Applied Physics, Lett. 68, pp. 3680-3682, 1996.
- [9] J. S. Roberts; et al. *Quantum cascade lasers grown by metalorganic vapor phase epitaxy*. Applied Physics Letters, Volume 82, Number 24, 2003.
- [10] Jerome Faist; Federico Capasso; et al. *Quantum Cascade Laser*. Science, New Series, Vol. 264, No. 5158, 1994.
- [11] R. U. Martinelli; R. J. Menna; et al. *Mid-Infrared III-V Diode Lasers for Trace-Gas Sensing*. IEEE Journal, Volume 2, p.310 - 311, 1995.
- [12] Thierry Aellen; et al. *Continuous-wave distributed-feedback quantum-cascade lasers on a Peltier cooler*. Applied Physics Letters, Volume 83, Number 10, 2003.
- [13] Kenneth O. Hill and Gerald Meltz. *Fiber Bragg Grating Technology Fundamentals and Overview*. Journal Of Lightwave Technology, VOL. 15, NO. 8, 1997.
- [14] F. N. Hooge. *1/f noise sources*. IEEE Transactions on electron devices, VOL. 41 NO. 11, 1994.
- [15] Bell Laboratories. *Quantum Cascade Lasers*. Bell Laboratories, Lucent Technologies, <http://www.bell-labs.com/org/physicalsciences/projects/qcl/qcl.html>, 2000.
- [16] NEO monitors AS Lasergas. *LaserGas SP II monitor, User´s reference*. neo monitors AS, Solheimveien 62A, Lørenskog.
- [17] Randall K. Kirschman; John A. Lipa. *Further evaluation of GaAs FETs for cryogenic readout*. W. W. Hansen experimental physics laboratories, Stanford University, Stanford, California, 1993.

- [18] Kent H. Lundberg. *Noise sources in bulk CMOS*. Massachusetts institute of technology, 77 Massachusetts Avenue, Cambridge, 2002.
- [19] Clayton R. Paul. *Derivation of common impedance coupling from the transmission-line equations*. IEEE Transactions on electromagnetic compatibility, Vol. 34, NO. 3, 1992.
- [20] David M. Pozar. *Microwave and RF design of wireless systems*. John Wiley and sons, Inc., New York, 2001.
- [21] Carlo Beenakker; Schonenberger. *Quantum shot noise*. Physics today, P. 37, May.
- [22] Bjørn Sletbakk. *Quantum cascade laser for spectroscopic gas detection and laser driver construction*. NTNU, Norwegian university of science and technology, Trondheim, 2007.
- [23] Joar M. Østby. *Elektrisk støy, mottiltak og beregning*. NTNU, Norwegian university of science and technology, subject INF5460.
- [24] B.E.A. Saleh; M.C. Teich. *Fundamentals of Photonics*. John Wiley and Sons Inc., New York, 1991.
- [25] Brian M. Tissue. *Photodiode and Photovoltaic Detectors*. Electrochemistry Laboratory, <http://elchem.kaist.ac.kr/>, 1996.
- [26] Brian M. Tissue. *Beer-Lambert law*. Virginia Tech, <http://teaching.shu.ac.uk/hwb/chemistry/tutorials/molspec/beers1.htm>, 2000.
- [27] G. Wysocki.; A.A. Kosterev; F.K. Tittel. *Spectroscopic trace-gas sensor with rapidly scanned wavelengths of a pulsed quantum cascade laser for in situ NO monitoring of industrial exhaust systems*. Department of Electrical and Computer Engineering, Rice University, 6100 Main Street, Houston, TX 77251, USA, 2005.

A Datasheet for the QCL

Nanosystems and
Technologies
GmbH

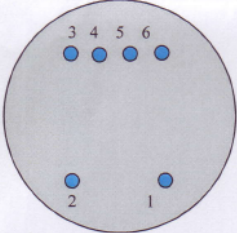


Datasheet for 7.42 μm DFB-Laser G2102/DFB2/5-12

(Device protected by US patent no. 6,671,306)

General

The Laser is mounted on TO8-header. On the header are the Thermo electric cooler (TEC) and NTC Thermistor. Electrical connections are as shown (back view):



Pin functions:

Pin No.	Function
1	TEC (-)
2	TEC (+)
3	Thermistor
4	Thermistor
5	LD (+)
6	LD (-)/ground

Caution: This device is susceptible to damage as a result of electrostatic discharge, high temperature, and mechanical forces. Proper precautions should be taken during both testing and handling. The maximum operation current is 2.8 A.

Warning: Invisible laser radiation. Avoid eye or skin contact to direct or scattered radiation.

NTC and TEC

Resistance R for different temperatures T(K) according to:

$$R=R_0 \cdot \exp[B(1/T-1/T_0)]$$

with

To 25 °C (= 298.15 K)
Ro 10000 Ohm
B 3600 K

TEC specification

$\Delta\Delta T_{\text{max}}$ = 72 K
Imax = 0.5 A
Umax = 2.2 V
Qmax = 1.45 W

Caution: Before operating the cooler: TO8 has to be connected to a heat sink.

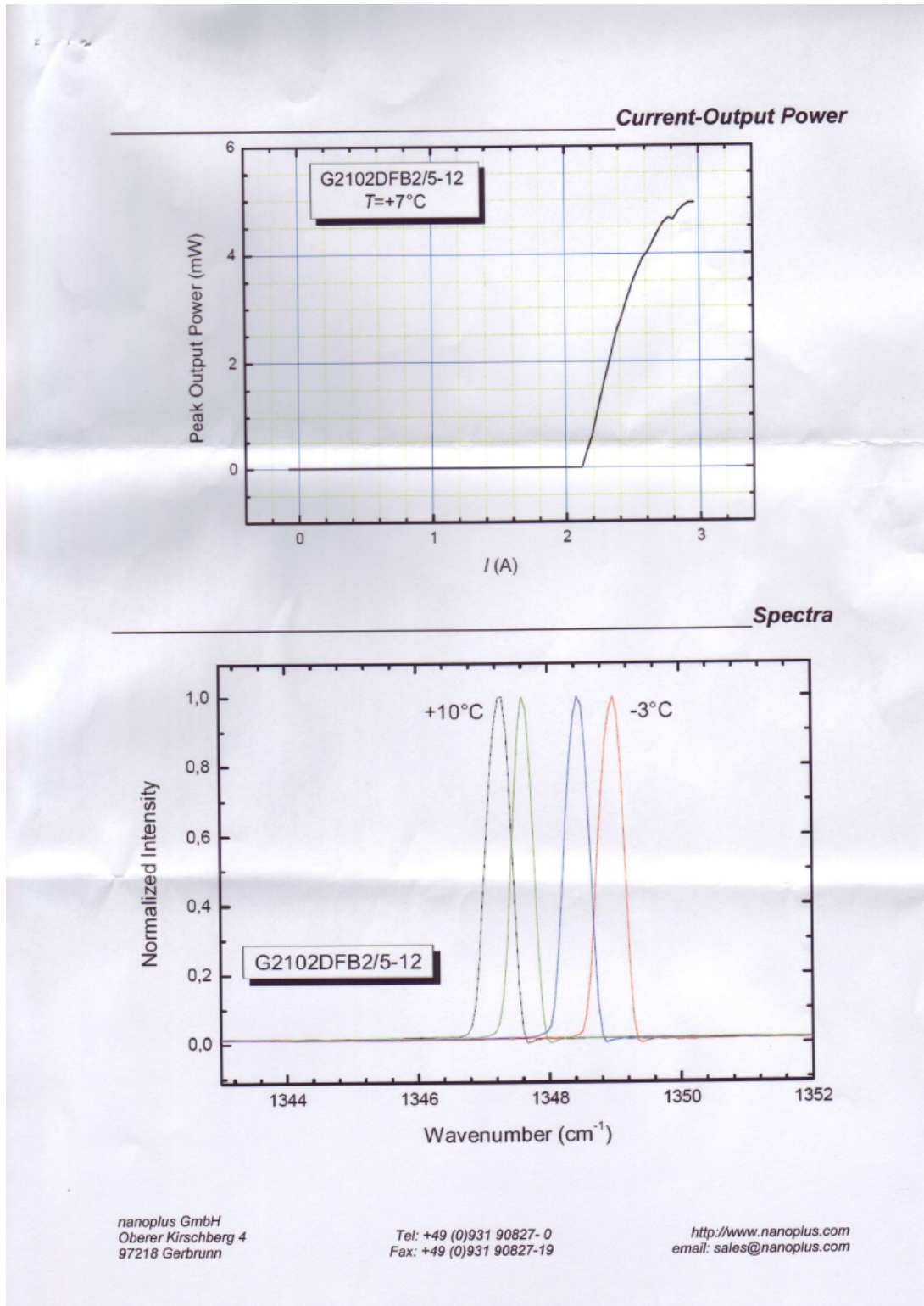
Laser Safety Information

Class 1m Laser Product
Do not view directly with optical instruments

nanoplus GmbH
Oberer Kirschberg 4
97218 Gerbrunn

Tel: +49 (0)931 90827-0
Fax: +49 (0)931 90827-19

<http://www.nanoplus.com>
email: sales@nanoplus.com



Operation Parameters

Laser Nr.	G2102/DFB2/5-12
wavelength	7.42 μm
output power	4 mW
temperature	7°C
pulse width	100 ns
repetition rate	1 kHz
threshold current	2.15 A @ 7°C
slope efficiency	8.9 mW/A @ 7°C
operation current	2.6 A
max. current	2.8 A
wavelength tuning	0.5 nm/A 0.6 nm/°C

B Datasheet for the Vigo detector

TEST of VIGO PHOTODETECTORS			
DETECTOR DESCRIPTION		MEASURED	
Manufacturer	Vigo System S.A.	Resistance	
Detector Type	PVI-2TE-8	Thermistor Resistance	
Active Area, mm ²	1	Spectral response using	MIR8000 FTIR
Window	BaF ₂		
Contract	10265179/6.0248		
TEST CONDITIONS		CALCULATED	
Ambient Temperature, K:	293	Responsivity	
Cooler Current I _{max} , A:	1.4	Noise Density	
Cooler Current I _{opt} , A:	1.2	Detectivity	
Cooler Voltage, V:	1.3		
Responsivity and Detectivity measurement accuracy 20% or better			
TEST RESULTS			
	UNITS	No	
		4141	
RESPONSIVITY (8μm)	A/W	1.25	
NOISE DENSITY	pA/Hz ^{1/2}	22.1	
DETECTIVITY (8μm)	cmHz ^{1/2} /W	5.7E+09	
DETECTOR RESISTANCE	Ω	26	
DETECTOR TEMPERATURE	K	216	
THERMISTOR RESISTANCE	kΩ	80	
THERMISTOR TYPE TB06-22			
FOR MORE INFORMATION ON THESE AND OTHER VIGO-SYSTEM PRODUCTS, PLEASE CONTACT US			
VIGO SYSTEM S.A.			
3 Światlików Str., 01- 389 Warsaw, Poland		e-mail info@vigo.com.pl.	
Tel: (4822) 6661410, (4822) 6660145		Fax: (4822) 6652155, (4822) 6660159	

TEST OPERATOR A.Mrówczyńska

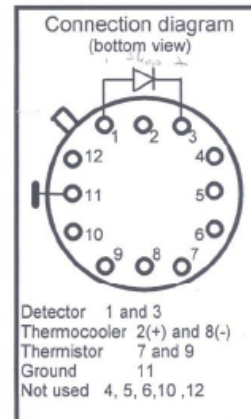
DATE: 13.09.2006

QUALITY CONTROL Z.Orman

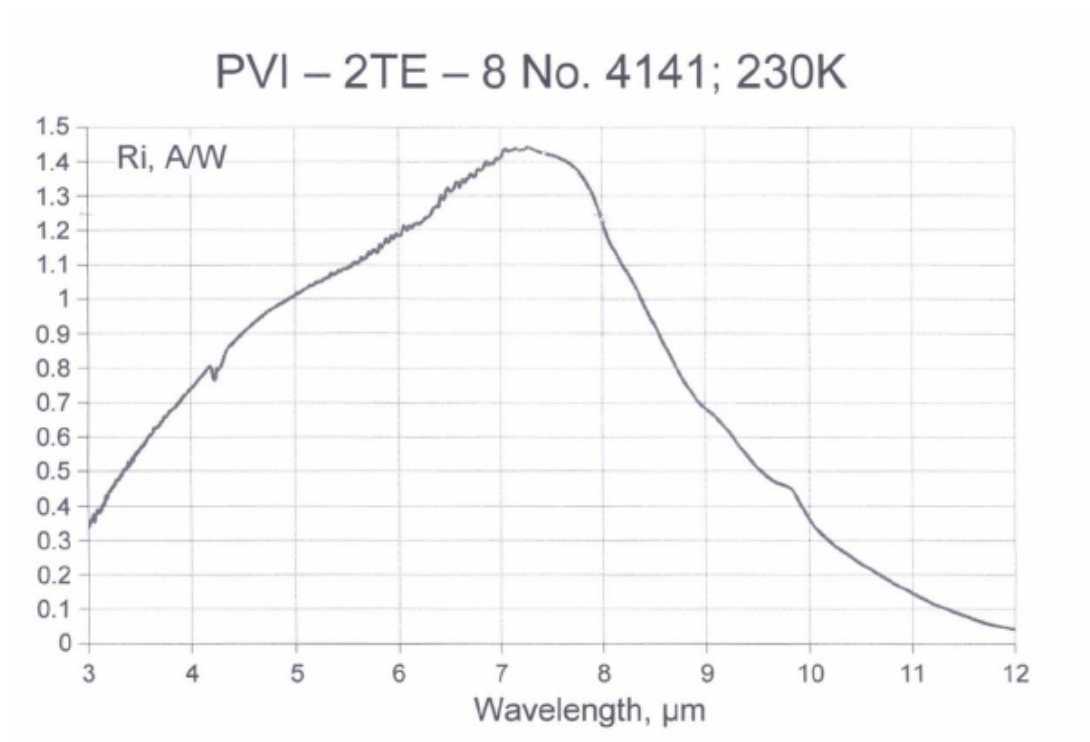
DATE: 13.09.2006

Warning

Electrostatic discharges may easily damage the device!
The electrical leads to the detector should be shorted during
storage and mounting! The electrostatic discharge threat
is especially serious in dry atmosphere!



Thermistor resistance (TB06-22) vs temperature							
T, K	T, °C	R, kΩ	±5%, -5%	T, K	T, °C	R, kΩ	±5%, -5%
190	-83	487.44	24.37	267	-6	5.804	0.290
192	-81	415.35	20.77	269	-4	5.351	0.268
194	-79	355.10	17.75	271	-2	4.939	0.247
196	-77	304.56	15.23	273	0	4.564	0.228
198	-75	262.02	13.10	275	2	4.223	0.211
200	-73	226.11	11.31	277	4	3.911	0.196
202	-71	195.68	9.78	279	6	3.627	0.181
204	-69	169.83	8.49	281	8	3.367	0.168
206	-67	147.81	7.39	283	10	3.128	0.156
208	-65	128.98	6.45	285	12	2.910	0.145
210	-63	112.84	5.64	287	14	2.709	0.135
212	-61	98.98	4.95	289	16	2.525	0.126
214	-59	87.02	4.35	291	18	2.356	0.118
216	-57	76.70	3.83	293	20	2.200	0.110
218	-55	67.76	3.39	295	22	2.056	0.103
220	-53	59.99	3.00	297	24	1.924	0.096
222	-51	53.23	2.66	299	26	1.801	0.090
224	-49	47.34	2.37	301	28	1.688	0.084
226	-47	42.18	2.11	303	30	1.584	0.079
228	-45	37.66	1.88	305	32	1.487	0.074
230	-43	33.69	1.68	307	34	1.397	0.070
232	-41	30.20	1.51	309	36	1.313	0.066
234	-39	27.12	1.36	311	38	1.236	0.062
236	-37	24.40	1.22	313	40	1.164	0.058
238	-35	21.99	1.10	315	42	1.097	0.055
240	-33	19.86	0.99	317	44	1.035	0.052
242	-31	17.96	0.90	319	46	0.977	0.049
244	-29	16.27	0.81	321	48	0.923	0.046
246	-27	14.76	0.74	323	50	0.872	0.044
248	-25	13.41	0.67	325	52	0.825	0.041
250	-23	12.21	0.61	327	54	0.781	0.039
252	-21	11.13	0.56	329	56	0.740	0.037
254	-19	10.16	0.51	331	58	0.701	0.035
256	-17	9.28	0.46	333	60	0.665	0.033
258	-15	8.50	0.42	335	62	0.631	0.032
260	-13	7.79	0.39	337	64	0.599	0.030
262	-11	7.15	0.36	339	66	0.569	0.028
264	-9	6.57	0.33	341	68	0.541	0.027
266	-7	6.05	0.30	343	70	0.515	0.026



C Datasheet for the BCT03C6V2 Zener diode

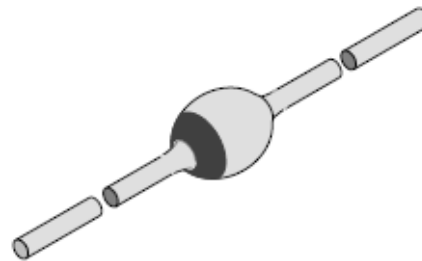


BZT03C...
Vishay Telefunken

Silicon Z-Diodes and Transient Voltage Suppressors

Features

- Glass passivated junction
- Hermetically sealed package
- Clamping time in picoseconds



94 9539

Applications

Medium power voltage regulators and medium power transient suppression circuits

Absolute Maximum Ratings

$T_J = 25^\circ\text{C}$

Parameter	Test Conditions	Type	Symbol	Value	Unit
Power dissipation	$l=10\text{mm}, T_L=25^\circ\text{C}$		P_V	3.25	W
	$T_{\text{amb}}=25^\circ\text{C}$		P_V	1.3	W
Repetitive peak reverse power dissipation			P_{ZRM}	10	W
Non repetitive peak surge power dissipation	$t_p=100\mu\text{s}, T_J=25^\circ\text{C}$		P_{ZSM}	600	W
Junction temperature			T_J	175	$^\circ\text{C}$
Storage temperature range			T_{stg}	-85...+175	$^\circ\text{C}$

Maximum Thermal Resistance

$T_J = 25^\circ\text{C}$

Parameter	Test Conditions	Symbol	Value	Unit
Junction ambient	$l=10\text{mm}, T_L=\text{constant}$	R_{thJA}	48	K/W
	on PC board with spacing 25mm	R_{thJA}	100	K/W

Electrical Characteristics

$T_J = 25^\circ\text{C}$

Parameter	Test Conditions	Type	Symbol	Min	Typ	Max	Unit
Forward voltage	$I_F=0.5\text{A}$		V_F			1.2	V

BZT03C...

Vishay Telefunken



Type BZT03C...	V _Z			r _z and TK _{vz} at I _Z				I _R at V _R		
	V	V	V	Ω	Ω	%/K	%/K	mA	μA	
	Min.	Typ.	Max.	Typ.	Max.	Min.	Max.		Max.	
6V2	5.8	6.2	6.6	1	2	0	0.07	100	1500	4.7
6V8	6.4	6.8	7.2	1	2	0	0.07	100	1000	5.1
7V5	7.0	7.5	7.9	1	2	0	0.07	100	750	5.6
8V2	7.7	8.2	8.7	1	2	0.03	0.08	100	600	6.2
9V1	8.5	9.1	9.6	2	4	0.03	0.08	50	20	6.8
10	9.4	10	10.6	2	4	0.05	0.09	50	10	7.5
11	10.4	10	11.8	4	7	0.05	0.10	50	4	8.2
12	11.4	12	12.7	4	7	0.05	0.10	50	3	9.1
13	12.4	13	14.1	5	10	0.05	0.10	50	2	10
15	13.8	15	15.6	5	10	0.05	0.10	50	1	11
16	15.3	16	17.1	6	15	0.06	0.11	25	1	12
18	16.8	18	19.1	6	15	0.06	0.11	25	1	13
20	18.8	20	21.2	6	15	0.06	0.11	25	1	15
22	20.8	22	23.3	6	15	0.06	0.11	25	1	16
24	22.8	24	25.6	7	15	0.06	0.11	25	1	18
27	25.1	27	28.9	7	15	0.06	0.11	25	1	20
30	28	30	32	8	15	0.06	0.11	25	1	22
33	31	33	35	8	15	0.06	0.11	25	1	24
36	34	36	38	21	40	0.06	0.11	10	1	27
39	37	39	41	21	40	0.06	0.11	10	1	30
43	40	43	46	24	45	0.07	0.12	10	1	33
47	44	47	50	24	45	0.07	0.12	10	1	36
51	48	51	54	25	60	0.07	0.12	10	1	39
56	52	56	60	25	60	0.07	0.12	10	1	43
62	58	62	66	25	80	0.08	0.13	10	1	47
68	64	68	72	25	80	0.08	0.13	10	1	51
75	70	75	79	30	100	0.08	0.13	10	1	56
82	77	82	87	30	100	0.08	0.13	10	1	62
91	85	91	96	60	200	0.09	0.13	5	1	68
100	94	100	106	60	200	0.09	0.13	5	1	75
110	104	110	116	80	250	0.09	0.13	5	1	82
120	114	120	127	80	250	0.09	0.13	5	1	91
130	124	130	141	110	300	0.09	0.13	5	1	100
150	138	150	156	130	300	0.09	0.13	5	1	110
160	153	160	171	150	350	0.09	0.13	5	1	120
180	168	180	191	180	400	0.09	0.13	5	1	130
200	188	200	212	200	500	0.09	0.13	5	1	150
220	208	220	233	350	750	0.09	0.13	2	1	160
240	228	240	256	400	850	0.09	0.13	2	1	180
270	251	270	289	450	1000	0.09	0.13	2	1	200


BZT03C...
Vishay Telefunken

Type	Clamping at		Stand-off at	
	$V_{(CLR)}^{1)}$ V	I_{RSM} A	I_R μA	$V_R^{2)}$ V
BZT03C...	Max.		Max.	
6V2	9.3	34.0	3000	5.1
6V8	10.2	31.0	2000	5.6
7V5	11.3	26.5	1500	6.2
8V2	12.3	24.4	1200	6.8
9V1	13.3	22.7	50	7.5
10	14.8	20.3	20	8.2
11	15.7	19.1	5	9.1
12	17.0	17.7	5	10
13	18.9	15.9	5	11
15	20.9	14.4	5	12
16	22.9	13.1	5	13
18	25.6	11.7	5	15
20	28.4	10.6	5	16
22	31.0	9.7	5	18
24	33.8	8.9	5	20
27	38.1	7.9	5	22
30	42.2	7.1	5	24
33	46.2	6.5	5	27
36	50.1	6.0	5	30
39	54.1	5.5	5	33
43	60.7	4.9	5	36
47	65.5	4.6	5	39
51	70.8	4.2	5	43
56	78.6	3.8	5	47
62	86.5	3.5	5	51
68	94.4	3.2	5	56
75	103.5	2.9	5	62
82	114	2.6	5	68
91	126	2.4	5	75
100	139	2.2	5	82
110	152	2.0	5	91
120	167	1.8	5	100
130	185	1.6	5	110
150	204	1.5	5	120
160	224	1.3	5	130
180	249	1.2	5	150
200	276	1.1	5	160
220	305	1.0	5	180
240	336	0.9	5	200
270	380	0.8	5	220

¹⁾ 10/1000 exp. falling pulse $t_p = 1000 \mu s$ down to 50%

BZT03C...

Vishay Telefunken



Characteristics ($T_j = 25^\circ\text{C}$ unless otherwise specified)

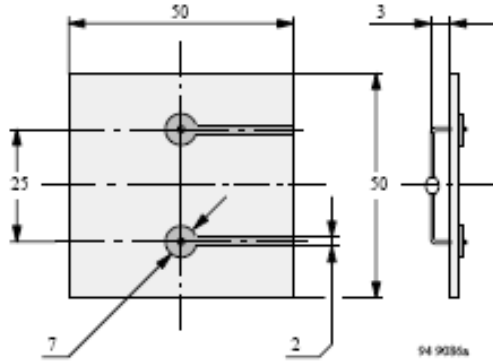


Figure 1. Epoxy glass hard tissue, board thickness 1.5 mm, $R_{thJA} \leq 100 \text{ K/W}$

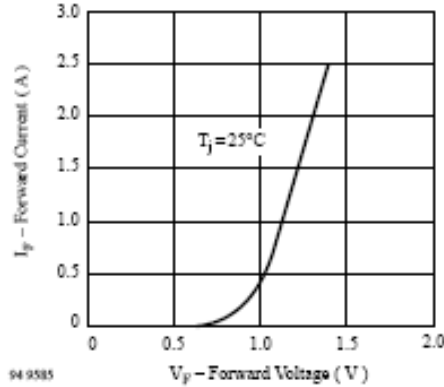


Figure 3. Forward Current vs. Forward Voltage

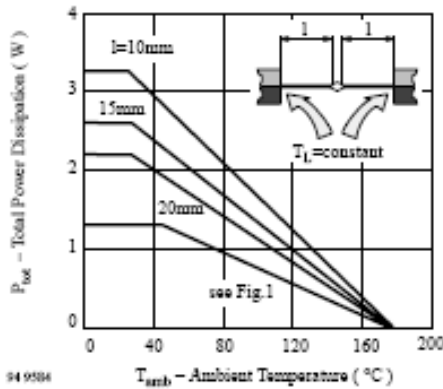


Figure 2. Total Power Dissipation vs. Ambient Temperature

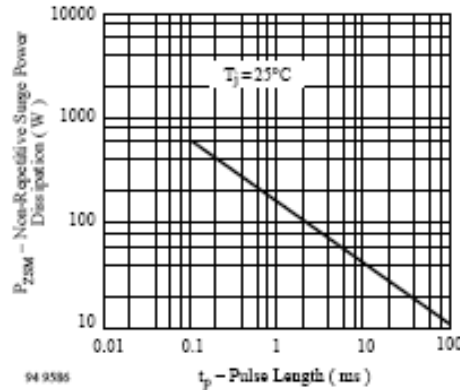
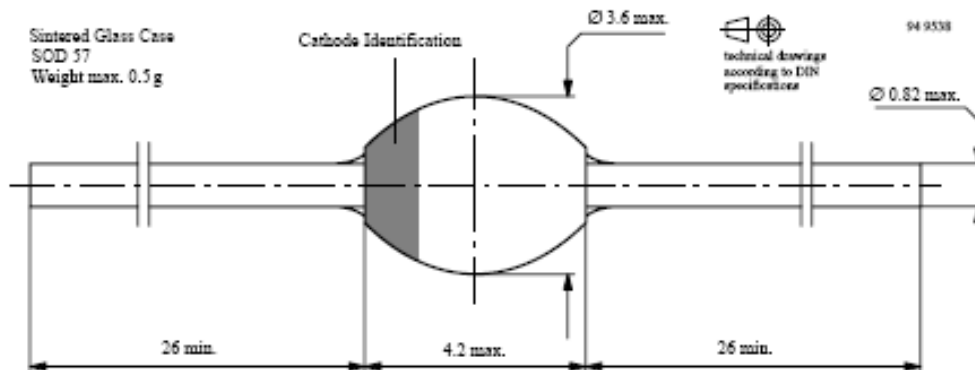


Figure 4. Non Repetitive Surge Power Dissipation vs. Pulse Length

Dimensions in mm





BZT03C...
Vishay Telefunken

Ozone Depleting Substances Policy Statement

It is the policy of Vishay Semiconductor GmbH to

1. Meet all present and future national and international statutory requirements.
2. Regularly and continuously improve the performance of our products, processes, distribution and operating systems with respect to their impact on the health and safety of our employees and the public, as well as their impact on the environment.

It is particular concern to control or eliminate releases of those substances into the atmosphere which are known as ozone depleting substances (ODSs).

The Montreal Protocol (1987) and its London Amendments (1990) intend to severely restrict the use of ODSs and forbid their use within the next ten years. Various national and international initiatives are pressing for an earlier ban on these substances.

Vishay Semiconductor GmbH has been able to use its policy of continuous improvements to eliminate the use of ODSs listed in the following documents.

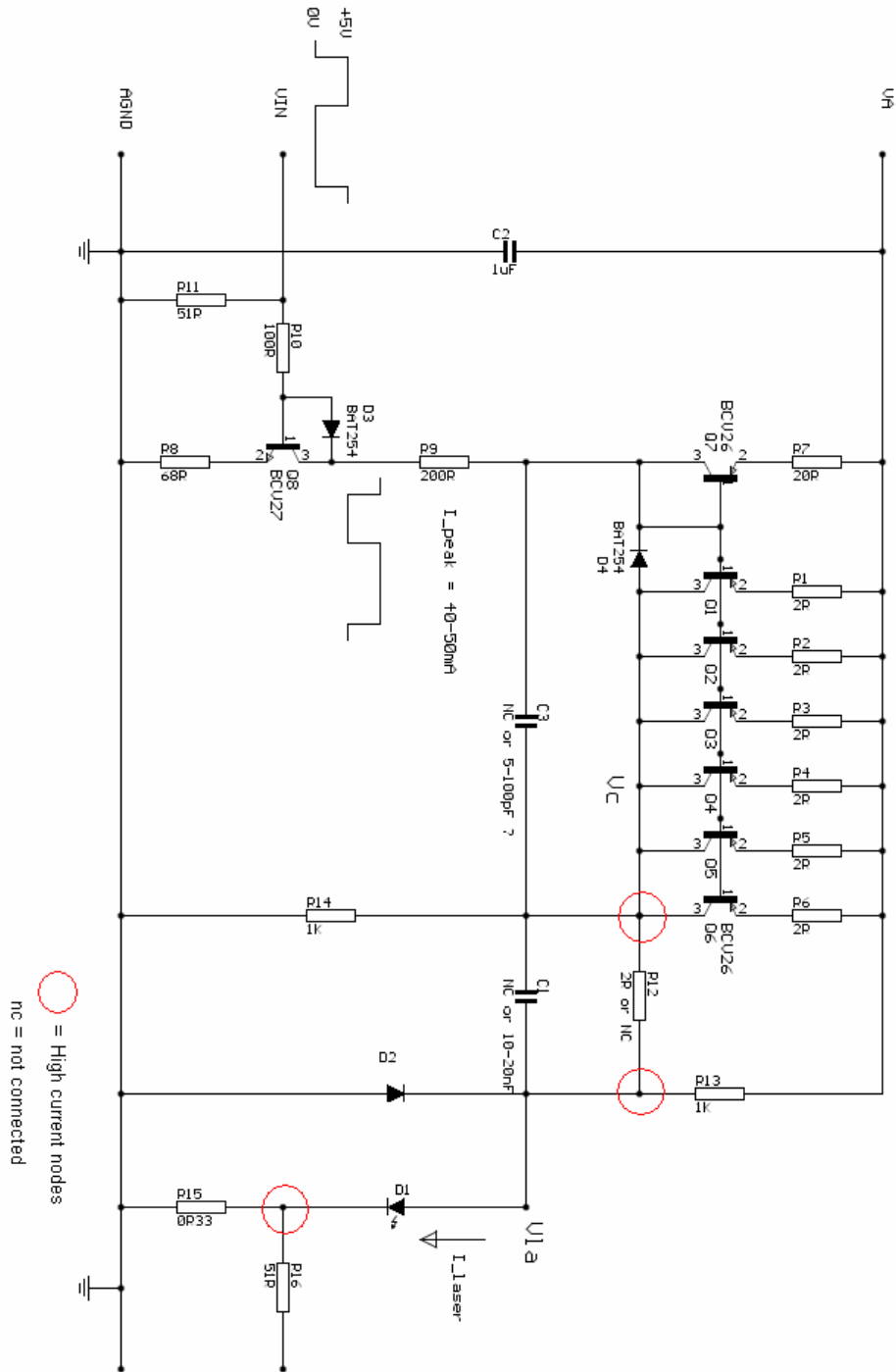
1. Annex A, B and list of transitional substances of the Montreal Protocol and the London Amendments respectively
2. Class I and II ozone depleting substances in the Clean Air Act Amendments of 1990 by the Environmental Protection Agency (EPA) in the USA
3. Council Decision 88/540/EEC and 91/890/EEC Annex A, B and C (transitional substances) respectively.

Vishay Semiconductor GmbH can certify that our semiconductors are not manufactured with ozone depleting substances and do not contain such substances.

We reserve the right to make changes to improve technical design and may do so without further notice. Parameters can vary in different applications. All operating parameters must be validated for each customer application by the customer. Should the buyer use Vishay-Telefunken products for any unintended or unauthorized application, the buyer shall indemnify Vishay-Telefunken against all claims, costs, damages, and expenses, arising out of, directly or indirectly, any claim of personal damage, injury or death associated with such unintended or unauthorized use.

Vishay Semiconductor GmbH, P.O.B. 3535, D-74025 Heilbronn, Germany
Telephone: 49 (0)7131 87 2831, Fax number: 49 (0)7131 87 2423

D NEO design driver module circuit



E PCO 7120 information

Specifications

PARAMETER	VALUE
Output Current	5A to 50A, controlled by input high voltage amplitude
Minimum Pulse Width (Typical)	12ns (12E-9S)
Maximum Pulse Width with 5% Pulse Droop	1 μ s (1E-6S) @ 50A, 10 μ s (10E-6S) @ 5A
Pulse Rise Time (10% to 90%) (Typical)	8ns (8E-9S)
PRF (Pulse Recurrence Frequency)	Single Shot to 1MHz, limited by maximum average current, controlled by input gate frequency (see table and graph below)
Gate Input	+5V into 50 Ω , Output pulse width and freq. follow input gate width and freq.
Output Current Monitor	20A/V into 50 Ω
Support Power	+12VDC to +15VDC at 60mA typical
DC HV Input	5V to 100V, Output current amplitude controlled by input DC voltage amplitude
Throughput (Propagation) Delay	<40ns, typically 36ns
MECHANICAL	
Size	Driver Only: 51mm (2.00") W x 82.5mm (3.25") L x 13mm (0.51") H Driver and Heatsink: 51mm (2.00") W x 103mm (4.06") L x 19.3mm (0.76") H
Weight	Driver Only: 35g (1.22oz) Driver and Heatsink: 128g (4.5oz)
Operating Temperature	-20C to +55C
ALL SPECIFICATIONS MEASURED INTO A SHORTED OUTPUT. SPECIFICATIONS SUBJECT TO CHANGE WITHOUT NOTICE.	

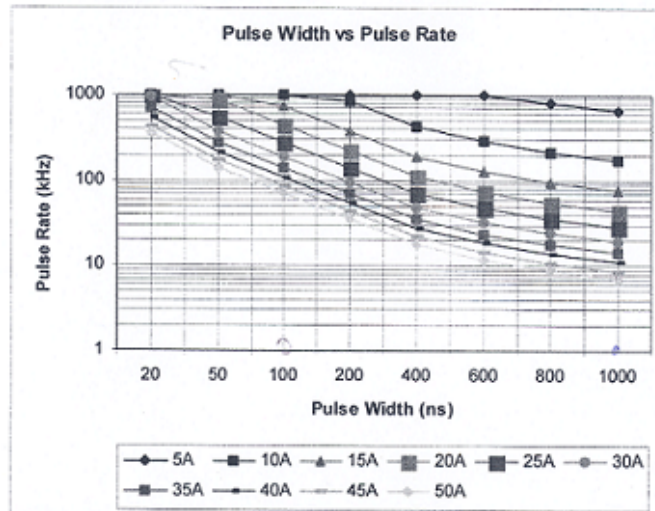


Figure 1 – Maximum Pulse Width vs Maximum Frequency

Output Current (A)	Maximum Duty Cycle	Typical DC HV Input (VDC)
5	0.65	10
10	0.17	18
15	0.075	26
20	0.045	34
25	0.028	42
30	0.019	51
40	0.011	70
50	0.007	92

Table 1 – Output Current vs Maximum Duty Cycle and Typical Input DC High Voltage

Please note that the typical DC HV input voltages in the table above are driving a shorted output. The laser diode forward voltage and the voltage required to overcome the laser diode and interconnect inductance must be taken into account in order to better approximate the actual voltage requirements. See "System Series Inductance" under the "Design Considerations" section below for additional detail.

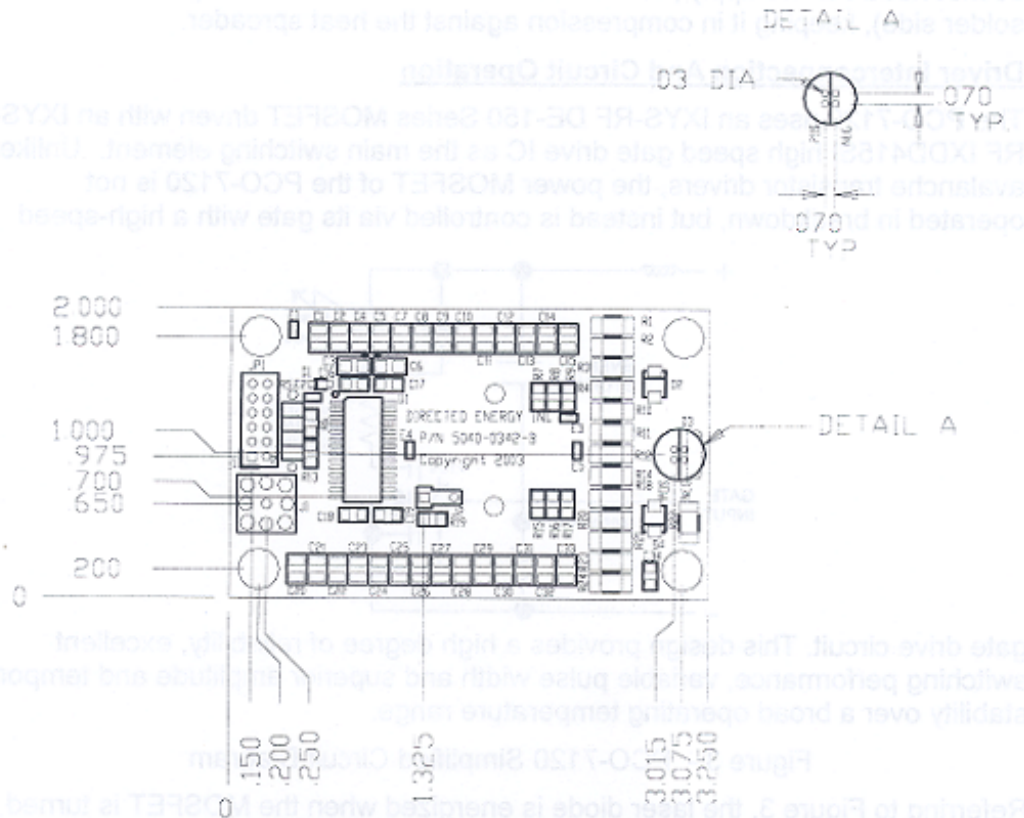


Figure 2A – PCO-7120 Dimensional Drawing – Circuit Board Only

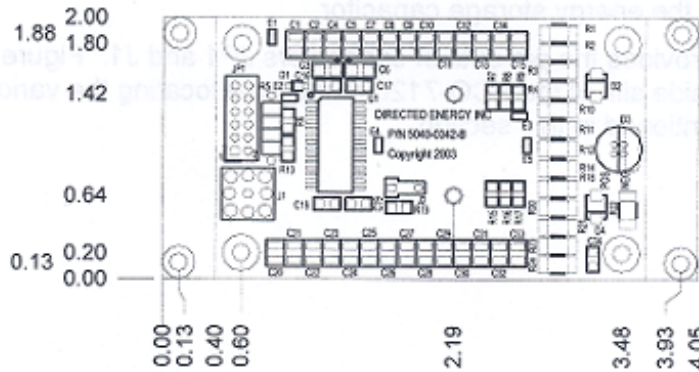


Figure 2B – PCO-7120 Dimensional Drawing With Heat Spreader

The circuit board is mounted to the heat spreader through the four mounting holes in the corners on 0.125" standoffs. The standoffs maintain the appropriate spacing between the circuit board and the heat spreader to accommodate the components mounted on the back (solder side) of the circuit board. The two

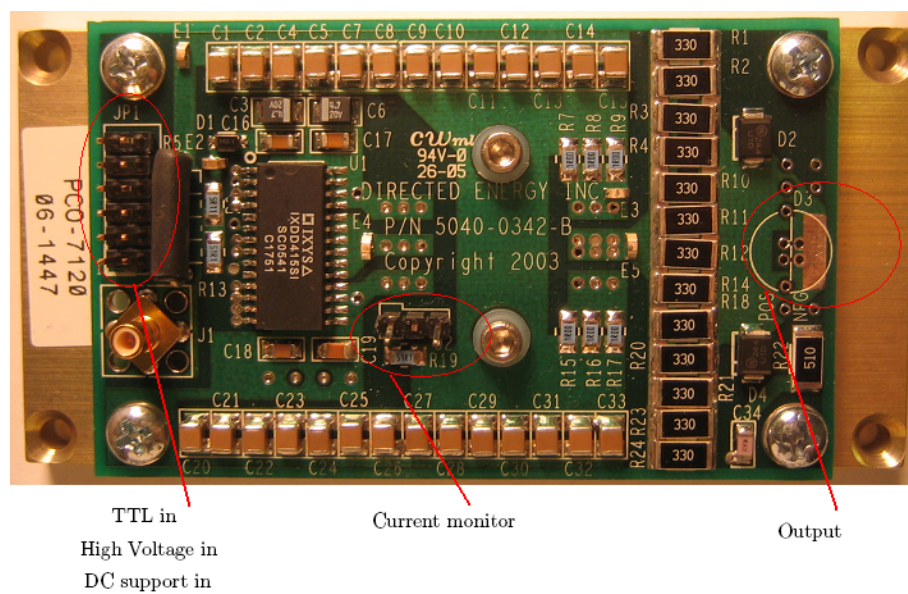


Figure E.37: Image of the PCO 7120 and its input and output terminals.

F Additional images of zener equivalent measurements



Figure F.38: Zener mounted on PCB. Current peak of 2.2 A

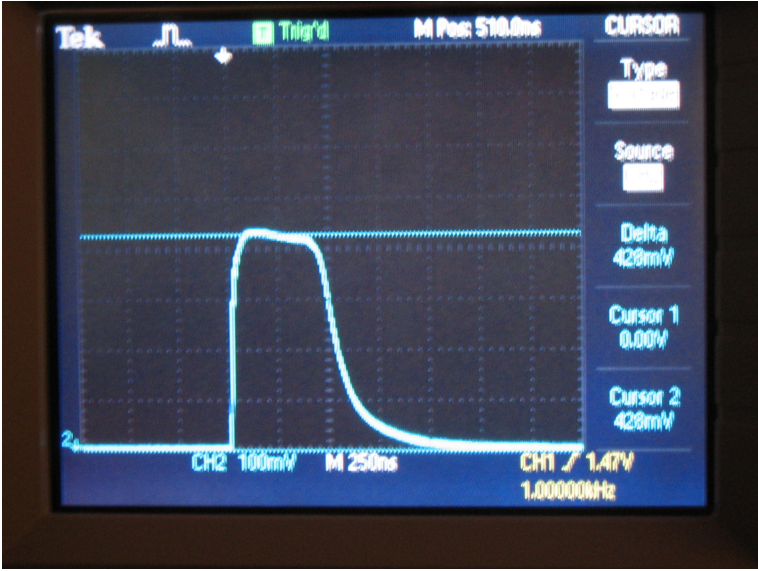


Figure F.39: Zener mounted on PCB. Current peak of 2.6 A



Figure F.40: Zener mounted with TP wires. Current peak of 2.2 A

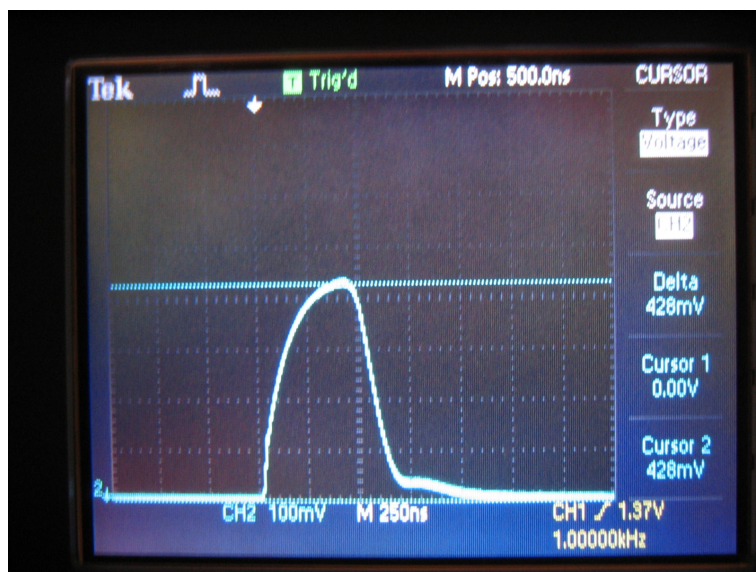


Figure F.41: Zener mounted with TP wires. Current peak of 2.6 A

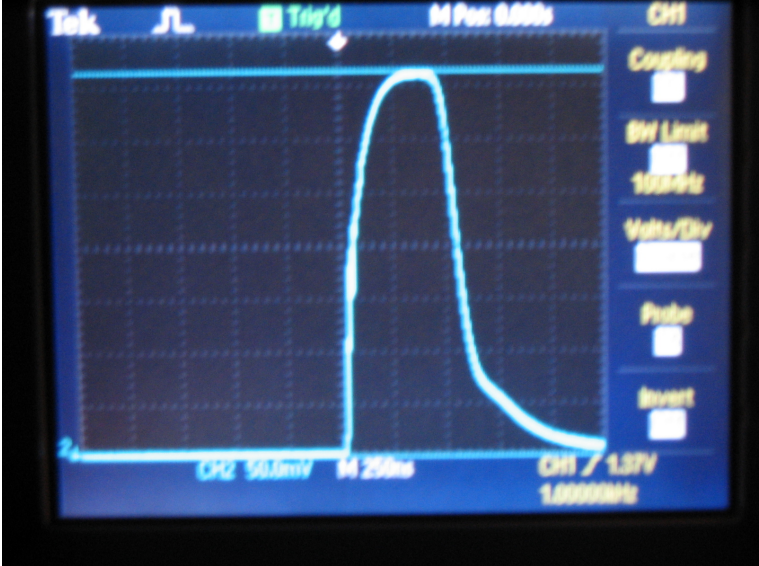


Figure F.42: Zener mounted with copper strip. Current peak of 2.2 A

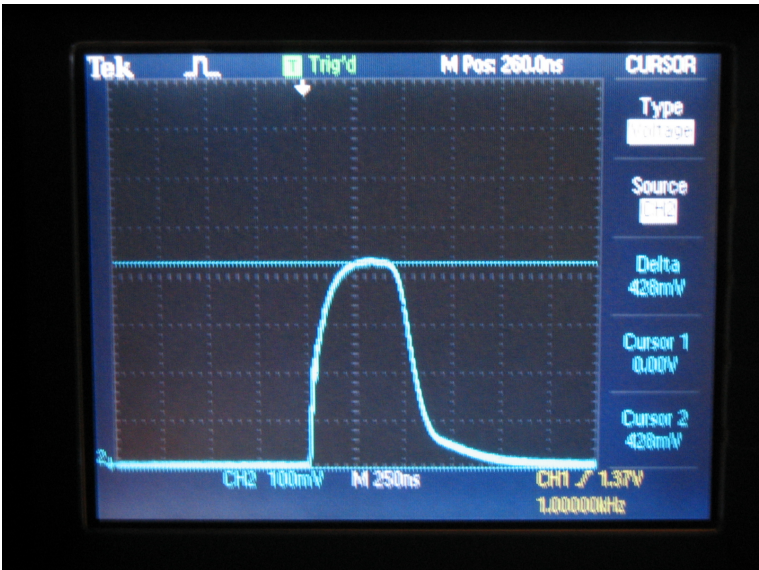


Figure F.43: Zener mounted with copper strip. Current peak of 2.6 A

G Comparison of I-V graphs for zener equivalent

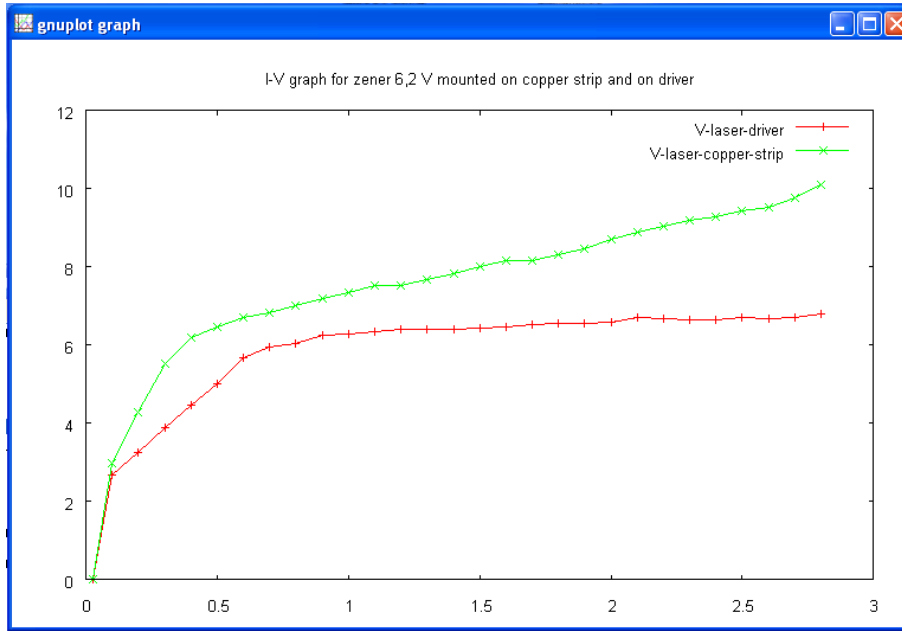


Figure G.44: Comparison of I-V graphs for zener mounted on PCB and on copper strip.

H Laboratory setup image

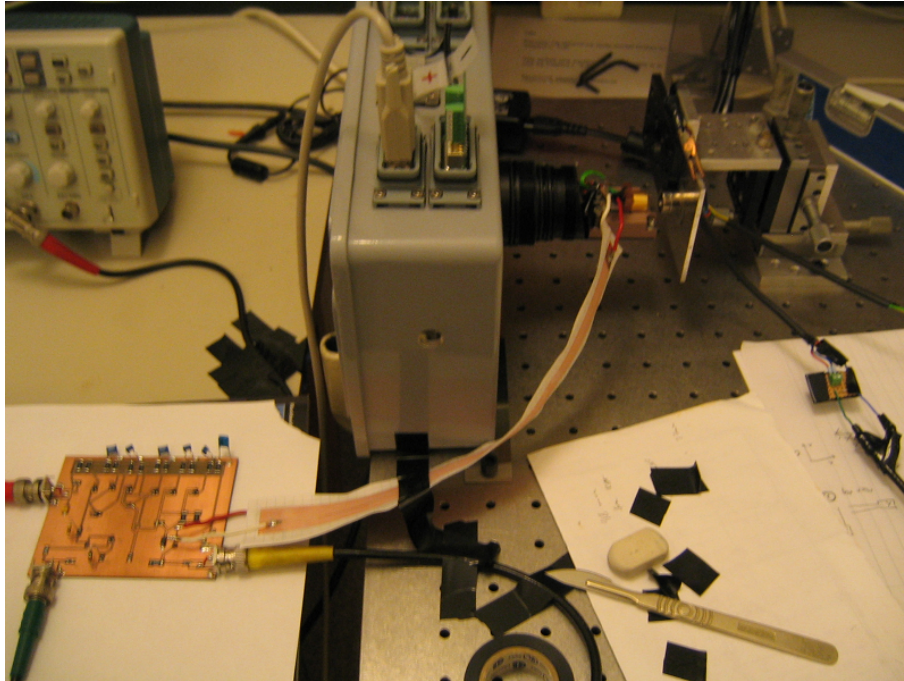


Figure H.45: Picture of the laboratory setup with detector close to QCL mount and aluminium tube removed.

I Noise measurements

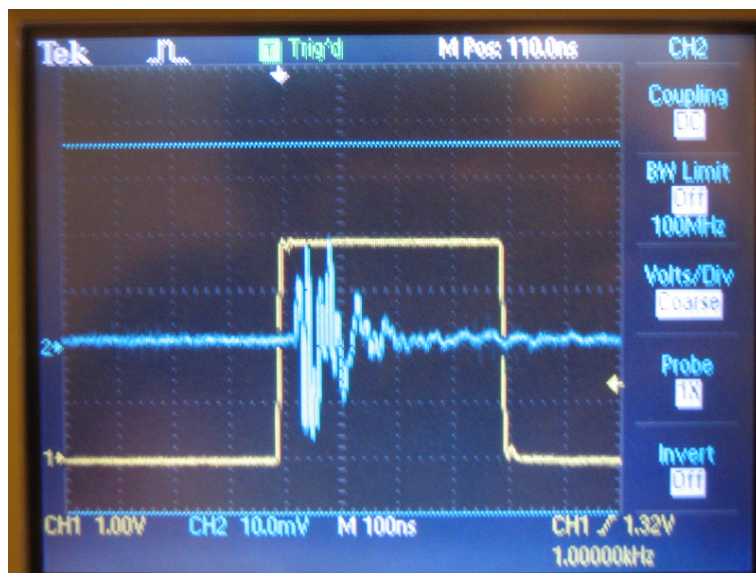


Figure I.46: Image of detector noise. Also showing the triggering signal of the detector.

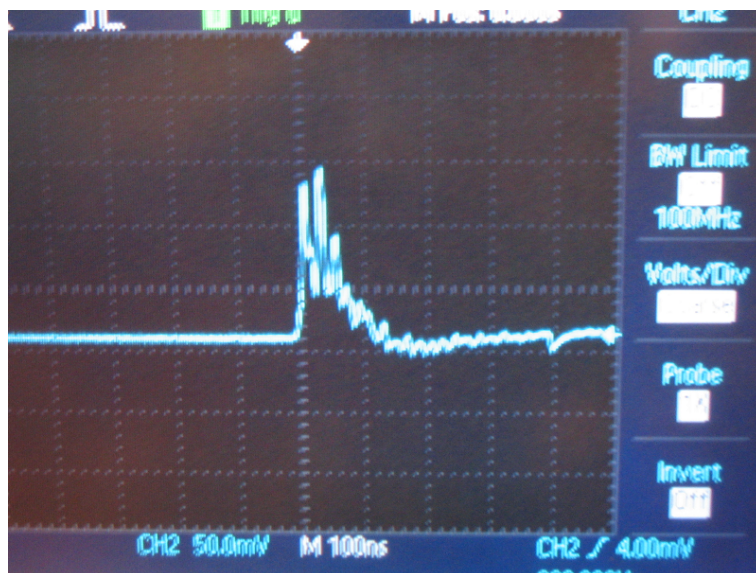


Figure I.47: Fluctuation in ground potential on PCB.

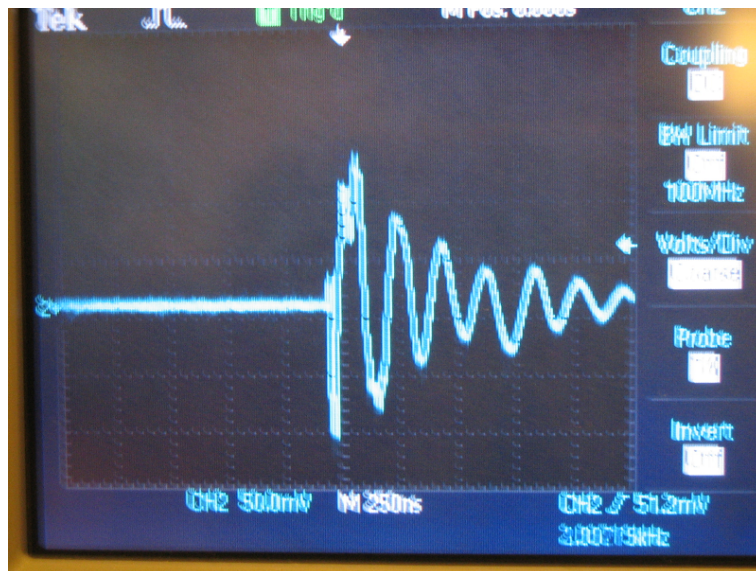


Figure I.48: Fluctuation in ground potential on PCB.

J Labview block diagram

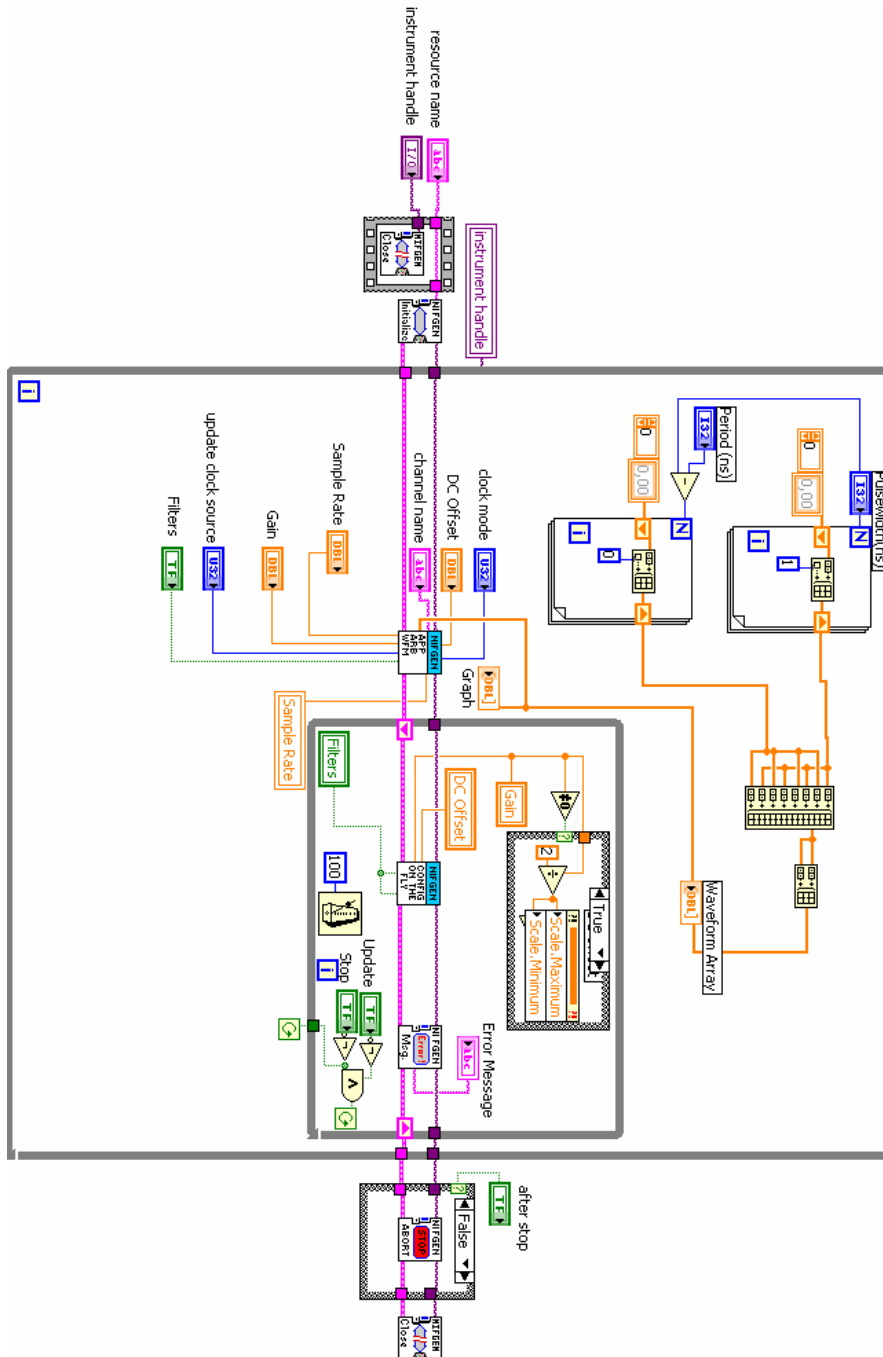


Figure J.49: The Labview block diagram used for pulse generation.